Color Tuning of Efficient Electroluminescence in the Blue and Green Regions Using Heteroleptic Iridium Complexes with 2-Phenoxyoxazole Ancillary Ligands

Helen Benjamin,[†] Jie Liang,[§] Yu Liu,*[,§] Yun Geng,[‡] Xingman Liu,[‡] Dongxia Zhu,*[,‡] Andrei S. Batsanov,[†] and Martin R. Bryce*[,†]

[†]Department of Chemistry, Durham University, Durham DH1 3LE, U.K.

[§]State Key Laboratory of Supramolecular Structure and Materials, College of Chemistry, Jilin University, Changchun 130012, P.R. China.

[‡]Key Laboratory of Nanobiosensing and Nanobioanalysis at Universities of Jilin Province, Department of Chemistry, North-east Normal University, 5268 Renmin Street, Changchun, Jilin Province 130024, P.R. China

E-mails: m.r.bryce@durham.ac.uk; yuliu@jlu.edu.cn; zhudx047@nenu.edu.cn
Supporting Information Placeholder

ABSTRACT: A rational molecular design strategy for tuning the emission color of phosphorescent complexes by functionalization of the bis-(2-phenylpyridine)(2-(2′-oxyphenyl)-2-oxazoline/oxazole)iridium(III) framework is reported. Five new complexes **2-6** have been synthesized in good yields and characterized by cyclic voltammetry, absorption and photoluminescence studies, by time-dependent density functional theory (TD-DFT) calculations, and single-crystal X-ray diffraction studies for complexes **2**, **4** and **6**. An interesting feature of the complexes is that the HOMO is localized on the Ir d-orbitals and the phenoxylate part of the 'ancillary' ligand, while the LUMO is located on the pyridyl ring of the ppy ligands. A few other complexes containing 2'-oxyphenyl-2-oxazoline/oxazole ancillary ligands have been reported previously; however, until now there has not been a systematic investigation into manipulating this unusual frontier orbital distribution to tune the emissive properties. It is shown that exchanging the phenylpyridine (ppy) ligand for 2,4-difluoro-ppy gives a blue shift of 21-22 nm (from **1** to **2**, and from **4** to **5**) and the introduction of electron-withdrawing substituents (SO_2Me, CF_3) onto the phenoxylate ring of the (2′-oxyphenyl)-2-oxazole ligand results in a further blue shift of 13-20 nm. Combining these functionalizations gives sky-blue emission with λ_{max}^{PL} 476 and 479 nm for complexes **5** and **6** in dichloromethane solution. The solution quantum yields of all the complexes are within the range Φ_{PL} 0.42-0.73. The observed lifetimes (τ_{obs} = 1.52-3.01 μs) and spectral profiles are indicative of phosphorescence from a mixture of ligand-centered (LC) and MLCT excited states. (TD-)DFT calculations are in close agreement with the observed photophysical and electrochemical properties of the complexes. Phosphorescent organic light-emitting diodes (PhOLEDs) have been fabricated using complexes **2**, **3**, **5** and **6** as the emitter, doped in a 4,4′-bis(*N*-carbazolyl)biphenyl (CBP) host, giving efficient emission in the blue-green region. Notably, complex **5** gives λ_{max}^{EL} 480 nm with maximum brightness of 26150 cd m^{-2}.

INTRODUCTION

Luminescent transition metal complexes[1] are renowned for their applications in diverse areas such as biological probes,[2] responsive materials,[3] water splitting, ion sensors, solar cells, phosphorescent organic light-emitting diodes (PhOLEDs) and solid-state lighting. In the context of PhOLEDs[4] and lighting[5] iridium(III) complexes have been at the forefront of attention since the pioneering studies of Forrest et al,[6] due to their outstanding combination of properties, namely: (i) synthetic versatility, (ii) good stability and color-tunability, (iii) high phosphorescence quantum efficiency, (iv) relatively short excited-state lifetimes of a few microseconds, and (v) good thin film processability. For these applications, homoleptic [Ir(C^N)$_3$] and heteroleptic iridium(III) complexes [Ir(C^N)$_2$L], are typically based on cyclometalated 2-phenylpyridine (ppy) ligands

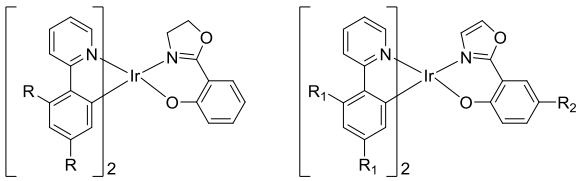

1 R = H
2 R = F
3 R_1 = H, R_2 = H
4 R_1 = H, R_2 = SO_2Me
5 R_1 = F, R_2 = SO_2Me
6 R_1 = F, R_2 = CF_3

Figure 1. Chemical structures of the oxazoline (**1**, **2**) and oxazole complexes (**3**-**6**).

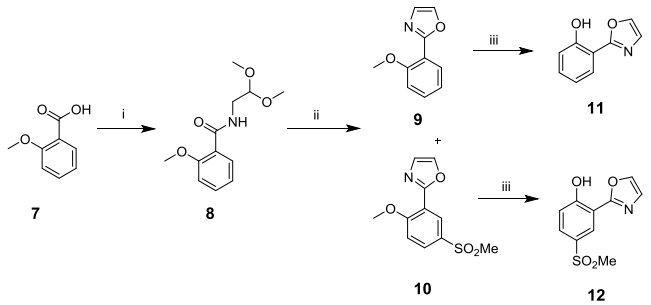

Scheme 1. Synthesis of ancillary ligands **11** and **12**. Reagents and conditions: (i) aminoacetaldehyde diethylacetal, 160 ^{o}C, (ii) $MeSO_3H/P_4O_{10}$, 180 ^{o}C, (iii) BBr_3, 0 ^{o}C, DCM

where the highest occupied molecular orbital (HOMO) is primarily localized on the iridium d-orbitals and the phenyl ring, while the lowest unoccupied molecular orbital (LUMO) is predominantly located on the pyridyl ring.[7] Emission is generally from a mixture of triplet metal-to-ligand charge-transfer (^{3}MLCT) states and $\pi-\pi^*$ transitions within the ligands. Electron-withdrawing groups on the phenyl ring of ppy lower the HOMO level while electron-donating groups on the pyridyl ring increase the LUMO level.[8] Varying the ancillary ligand in heteroleptic complexes, e.g. L = acetylacetonate,[9] picolinate,[10] bis(pyrazolyl)borate[11] or pyridylazolate,[12] is also an established strategy for color tuning of emission by perturbing the MLCT interaction. In some complexes interligand energy transfer can occur from the cyclometalating ppy ligand to the ancillary ligand, e.g. with a quinoline carboxylate ancillary ligand.[13]

We recently reported that complex **1** (Figure 1) featuring a 2'-oxyphenyl-2-oxazoline ancillary ligand showed promising green PhOLED performance, and, in particular, displayed an interesting distribution of the frontier orbitals.[14] The LUMO of **1** is located on the pyridyl ring of the ppy ligands, while the HOMO is localized on the Ir d-orbitals and the phenoxylate part of the 'ancillary' ligand.[14] A few other complexes containing 2'-oxyphenyl-2-oxazoline/oxazole ancillary ligands have been reported.[15] However, there is a lack of systematic investigation into manipulating this unusual frontier orbital distribution to tune the emissive properties.

In this work we focus on the synthesis, photophysical and electrochemical properties of five new iridium(III) complexes **2-6**, each with an oxazoline or oxazole ancillary ligand. Our targets were designed to utilize the unusual HOMO-LUMO distribution to blue shift the emission relative to complex **1**. We have successfully achieved this via simple and rational substitutions on both the phenylpyridine and the ancillary ligands. It is well documented in the literature that introducing electron-withdrawing groups, such as fluorine,[11] perfluoroalkyl,[16] sulfonyl,[17,18] phosphoryl,[17] and cyano substituents, onto positions of HOMO localization is an effective method to blue shift the emission of the resultant iridium complex. With this in mind we introduced SO_2Me and CF_3 groups *para* to the hydroxyl on the 2-(2´-oxyphenyl)-2-oxazole ligand with the aim of lowering the HOMO. Fluorine substituents were also introduced on the ppy ligands, even though they have little contribution to the HOMO in **1**, as it was thought they could blue-shift the emission by lowering the energy of the iridium d-orbitals, a strategy that is known for ancillary ligands.[10] PhOLED fabrication and efficient device performance in the blue-green region is reported for selected derivatives.

RESULTS AND DISCUSSION

Synthesis

The syntheses of the ancillary oxazole-based ligands and their derived complexes are shown in Schemes 1-3. All the complexes were characterized by NMR spectroscopy, mass spectrometry and elemental analysis, with X-ray crystal structures of complexes **2**, **4** and **6**. The synthesis of oxazoline ligand **21** (Scheme 3) is described in the literature.[14,19] The oxazole-containing ligand **11** was synthesized as shown in Scheme 1, via a condensation between carboxylic acid **7** and aminoacetaldehyde diethylacetal, followed by *in situ* deprotection of the masked aldehyde **8** and oxazole formation with Eaton's reagent. Two products were isolated, the desired compound **9**, and the methanesulfonyl derivative **10** (ca. 1:1 ratio). As we were interested in functionalizing the ancillary ligand, additional quantities of **10**, along with analog **19**, were synthesized as shown in Scheme 2, as it transpired that the route in Scheme 1 was not compatible with the desired substituents on the phenyl ring. The new route (Scheme 2) involved a condensation reaction between carboxylic acids **13** and **14** and aminoacetaldehyde diethylacetal to give **15** and **16**. The next step was a deprotection of the masked aldehyde with HCl to give **17** and **18**, followed by a cyclization with Burgess' reagent under microwave conditions,[20] to give ligand precursors **10** and **19**. The final step in both schemes was demethylation of **9**, **10** and **19**, which was achieved using either BBr_3 or pyridine.HCl, to afford the phenol derivatives **11**, **12** and **20**, respectively.

The new heteroleptic complexes **2-6** were then synthesized using standard conditions[21] (Scheme 3).

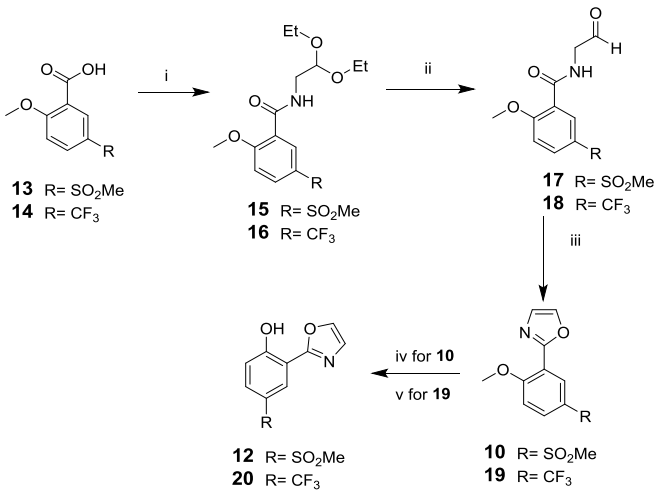

Scheme 2. Synthesis of ancillary ligands **12** and **20**. Reagents and conditions: (i) 1) $SOCl_2$, reflux, 2) aminoacetaldehyde diethylacetal, NEt_3, DCM, RT, (ii) catalytic HCl, acetone/water, reflux, (iii) Burgess' reagent, THF, microwaves, 70 ^{o}C, (iv) BBr_3, 0 ^{o}C, DCM, (v) pyridine.HCl, 160 ^{o}C

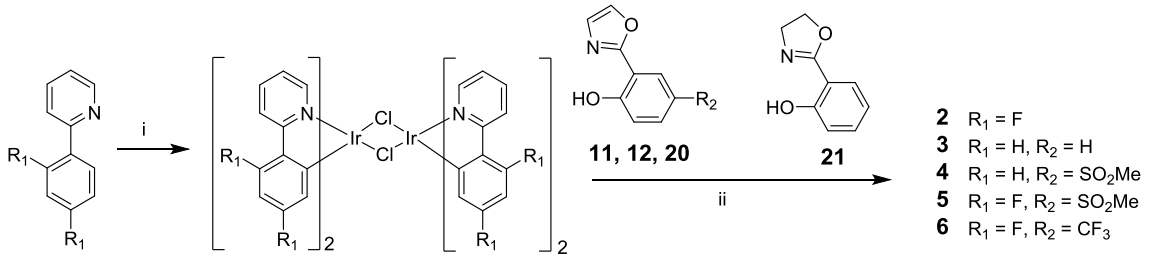

Scheme 3: Synthesis of complexes **2-6**. Reagents and conditions: (i) $IrCl_3.3H_2O$, 2-ethoxyethanol, 130 ^oC (ii) ancillary ligand **11**, **12**, **20** or **21**, Na_2CO_3, 2-ethoxyethanol, 130 ^oC

The intermediate μ-dichloro bridged dimer $[Ir(L)_2Cl]_2$ was reacted *in situ* with the appropriate ancillary ligand **11**, **12**, **20** or **21** in the presence of Na_2CO_3. The complexes **2-6** were obtained as yellow powders in 57-87% yields. The NMR spectra of **5** and **6** were obtained in acetone-d_6. This was because upon storage of the solutions of **5** and **6** in $CDCl_3$ under ambient conditions (laboratory light at 20 ^oC) partial re-formation of the dichloro bridged dimer was observed. This is ascribed to the presence of traces of acid, as noted by Baranoff *et. al.* for previous complexes.[22]

Thermal, Photophysical and Electrochemical Properties

The thermal stabilities of the iridium complexes were evaluated using thermogravimetric analysis (TGA) under a nitrogen atmosphere. The 5% weight loss temperatures (T_d) are above 300 °C for all complexes, suggesting the complexes should be thermally stable under device operation (Table S2).

The absorption and emission spectra of the complexes **2-6** in dichloromethane solutions are shown in Figure 2, and the data for **1-6** are listed in Table 1. The strong bands between 250-320 nm are assigned to π-π* transitions on the ligands based on literature precedents.[23] Absorption bands in the range of 350-460 nm with lower extinction coefficients are assigned to the ^{1}MLCT/^{3}MLCT bands following literature precedents,[18] and the calculations of Hay.[24] Emission from the complexes is in the green/blue-green region, and the following trends are observed. (i) Exchanging the oxazoline of the parent complex **1** for an oxazole (complex **3**) results in a small blue shift of 6 nm. This could be due to the increased electron withdrawing capability of the oxazole fragment, compared to the oxazoline, as a result of the extended conjugation.

(ii) Exchanging the ppy ligand for 2,4-difluorophenylpyridine gives a blue shift of 21-22 nm (from **1** to **2**, and from **4** to **5**) although computational data (see below) suggests the HOMO is localized on the phenoxylate of the ancillary ligand, not the phenyl of ppy. This change of emission color can be explained by the presence of two fluorines that could still influence the energy levels of the iridium d-orbitals, which are heavily involved in the excited state.

(iii) The introduction of electron-withdrawing moieties (SO_2Me, CF_3) onto the phenoxylate ring of the ancillary ligand results in a further blue shift of 13-20 nm. This was expected as the HOMO in the complexes is localized on that ring (see below).

(iv) The emission profiles of the complexes **2-4** is similar to that of the parent complex **1**[14], and are broad and largely featureless, indicating a strong MLCT contribution to the emission. However, for complexes **5** and **6** stronger vibronic features are observed as the emission is shifted further towards the blue, suggesting an increase in the LC contribution to the emission.[23,24]

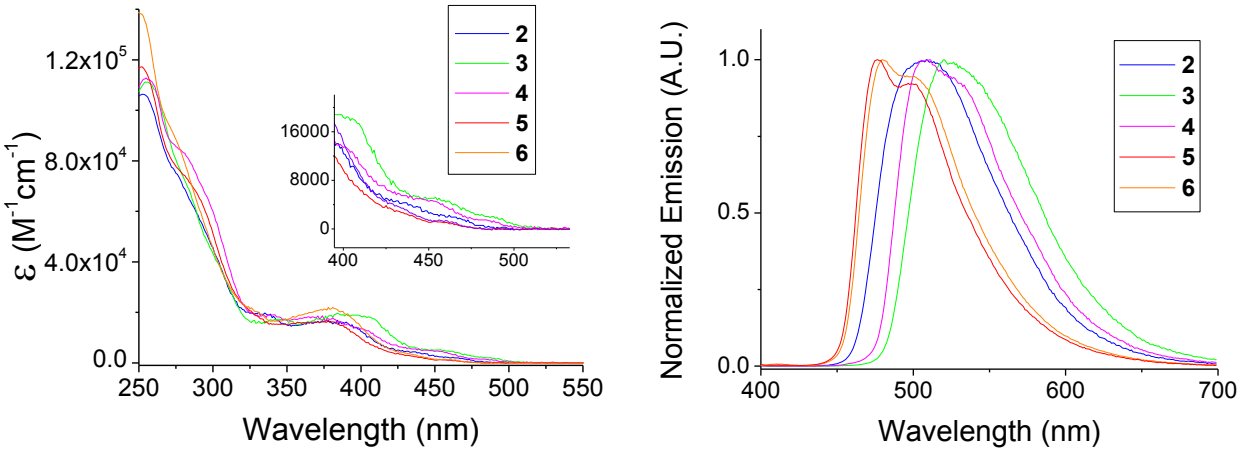

Figure 2. Absorption spectra of complexes **2-6** in DCM [<10^{-5} M]. Emission spectra of complexes **2-6** in degassed DCM [<10^{-5} M], λ_{ex} = 355 nm.

Table 1. Photophysical data for iridium complexes **1-6**.

Complex	λ_{max}^{abs} (ε) / nm (×10^3 M^{-1} cm^{-1})[a]	λ_{max}^{em} / nm[b]	PLQY / Φ_{PL}[a,c]	τ_P / μs[a,d]	k_r / 10^5 s^{-1}	k_{nr} / 10^5 s^{-1}	$E^{ox}_{1/2}$ / V[e]	HOMO / eV[f]	T_1 / eV[h]
1[g]	249, 340 (sh), 377 (sh), 443 (sh)	527	0.55	0.34	1.61	1.32	0.08	-4.88	2.51
2	252 (104.8), 275 (sh, 74.2), 334 (18.7), 374 (16.0), 390 (14.7), 438 (3.9), 464 (1.8)	506	0.65	1.52	4.28	2.30	0.37	-5.17	2.49
3	255 (119.3), 280 (sh, 79.3), 303 (sh, 43.3), 386 (20.8), 402 (18.5), 456 (5.2), 488 (2.0)	521	0.45	1.71	2.63	3.22	0.18	-4.98	2.57
4	253 (111.0), 279 (83.2), 297 (64.1), 339 (18.9), 365 (18.3), 380 (17.3), 401 (13.4), 451 (4.5), 483 (1.2)	508	0.42	1.80	2.33	3.22	0.30	-5.10	2.56
5	251 (118.6), 291 (65.5), 325 (20.6), 379 (16.2), 429 (3.5), 457 (1.4)	476, 501	0.73	3.01	2.43	0.90	0.76	-5.56	2.71
6	248 (140.3), 275 (89.9), 329 (20.3), 382 (20.7), 439 (2.6), 458 (1.2)	479, 502	0.69	2.95	2.34	1.05	0.72	-5.52	2.69

[a] Data obtained in dichloromethane solution at 20 °C. [b] Data obtained in degassed dichloromethane solution with λ_{ex} = 380 nm. [c] Measured in degassed DCM relative to quinine sulfate Φ_{PL}= 0.546 in 0.5 M H_2SO_4 at 20 °C; estimated error ±5%. [d] Estimated error ±5%.[e] All values are reported vs Fc/Fc^+ = 0.00 V. Measured in DCM (0.1 M $^nBu_4NPF_6$) at 298 K. [f] Obtained from the electrochemical oxidation potential. [g] Values for complex **1** taken from reference[12]. [h] Estimated from the onset wavelengths of the 77 K emission spectra measured in THF solution with λ_{ex} = 365 nm (Figure S38).

The photoluminescence quantum yields (PLQYs), lifetimes (τ_{obs}) and calculated radiative and non radiative decay rates (k_r and k_{nr}) are stated in Table 1. QYs are in the range Φ_{PL} 0.42-0.73. The observed lifetimes (τ_{obs} = 1.52−3.01 μs) are indicative of phosphorescence from a mixture of ligand-centered (LC) and MLCT excited states.6[b,25]

Electrochemistry

The electrochemical behavior of the complexes was investigated using cyclic voltammetry (CV) in a $^nBu_4NPF_6$ dichloromethane solution. All the complexes show an electrochemically quasi/irreversible oxidation at 0.08-0.76 V vs Fc/Fc^+, assigned to the Ir(III)/Ir(IV) couple (Table 1, Figure 3). Exchanging the ppy ligand for dfppy (**1** to **2**, and **4** to **5**) results in a large increase in the oxidation potential, of 0.29-0.46 V, indicating the fluorine substituents are efficient at lowering the HOMO. Introducing electron-withdrawing groups on the phenoxylate ring also increases the oxidation potential, (by 0.12 V for SO_2Me; compare **3** and **4**); this is consistent with the HOMO of **4** localized primarily on the phenoxylate ring of the ancillary ligand (see below) and introducing an electron-withdrawing group, such as a sulfone, should lower the HOMO level. Upon replacing the oxazoline fragment with an oxazole (**1** to **3**) the oxidation potential increases by 0.1 V. As the HOMO for **1** is localized on the iridium d-orbitals and across the phenoxylate ring it is possible that switching from an oxazoline to an oxazole lowers the HOMO energy due to the increased electron withdrawing ability of the oxazole compared to the oxazoline. If the LUMO energies are assumed to be very similar in these complexes, the relative HOMO energies from their CV data are consistent with the λ_{max} values obtained from the emission spectra (Table 1). No reduction features were observed within the solvent window (scanning to -1.5 V vs Fc/Fc^+).

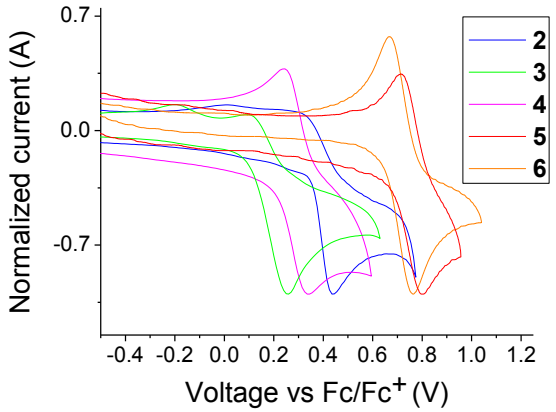

Figure 3. Cyclic voltammograms of complexes **2-6** measured in DCM (0.1 M $^nBu_4NPF_6$) at 298 K.

X-ray crystallography

Single crystal structures were obtained for **2**, **4** and **6**. In each case the Ir atom has a distorted octahedral coordination (Fig

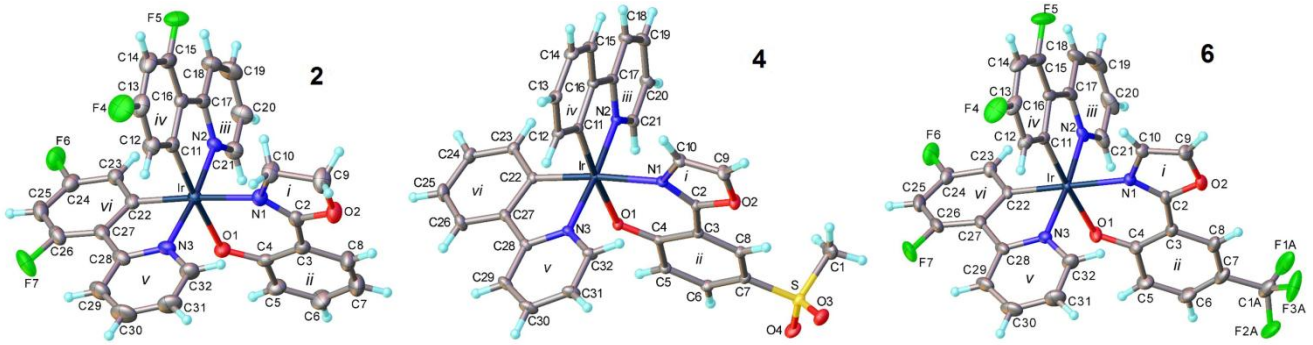

Figure 4. X-ray molecular structures of complexes **2**, **4** and **6**. The DCM (**2**), THF (**4**) and DCM/chloroform (**6**) molecules of crystallization and the disorder of the CF_3 group in **6** are not shown. Thermal ellipsoids are drawn at the 30% (**2**) or 50% (**4**, **6**) probability level.

ure 4). The 2-(2'-oxyphenyl)-2-oxazoline/oxazole ligand is chelating the metal via its oxy and N atoms. In **2** the oxazoline ring is planar, as in the non-coordinated molecule **21** in the crystal.[26] The twist between the oxazoline and benzene rings in **2** is 8.1°, whereas in **21** it is practically nil; planarity of **21** is stabilized by an intramolecular O-H…N bond. Nevertheless, the inter-ring bond C(2)-C(3) is shorter in **2** than in **21**, 1.442(6) vs 1.462(1) Å. The oxyphenyloxazole ligand in **4** and **6** is more planar and shows a stronger π-delocalisation in the chelate ring (Table 2). The C,N-chelating ppy ligands also show small but significant twists between the two aromatic systems. The Ir-C(11) bond, *trans* to the Ir-O(1), is shorter than the Ir-C(22) which is *trans* to the oxazole/oxazoline N(1), as expected from the *trans*-effect. The nitrogen atoms of these ligands are *trans* to each other; interestingly, in all three complexes the Ir-N(2) bond is slightly shorter than Ir-N(3), i.e. the Ir-N and Ir-C bonds in a chelate ring strengthen simultaneously.

The crystal packing of **2** shows intermolecular stacking between rigorously parallel rings *iii* and *v* and their respective inversion equivalents; the interplanar separations being *iii/iii'*3.57 and *v/v'* 3.60 Å. This may result in a continuous chain of π-π interactions. In **6** there is also a continuous chain through intermolecular stacking of moieties *iii* and *iv*, which are only approximately parallel (interplanar angle 11.4°, average separation 3.44 Å). The molecules of **4** form no such chain but a dimer through a tight π-π contact between inversion-related moieties *v* at 3.36 Å interplanar separation and 3.69 Å distance between ring centroids, which amounts to a 1.53 Å parallel slip of the rings along the N(3)…C(30) direction.

Table 2. Selected bond distances (Å) and interplanar angles (°) between mean ring planes

	2	4	**6**[a]	21
Ir-O(1)	2.134(3)	2.1452(8)	2.135(2)	
Ir-N(1)	2.119(3)	2.137(1)	2.126(2)	
Ir-N(2)	2.030(3)	2.035(1)	2.031(2)	
Ir-N(3)	2.040(4)	2.042(1)	2.041(2)	
Ir-C(11)	1.979(4)	1.989(1)	1.986(2)	
Ir-C(22)	2.001(4)	2.000(1)	2.001(2)	
N(1)-C(2)	1.292(6)	1.3116(15)	1.310(3)	1.283(1)
C(2)-C(3)	1.442(6)	1.4477(16)	1.443(3)	1.462(1)
C(3)-C(4)	1.415(6)	1.4333(16)	1.428(3)	1.410(1)
O(1)-C(4)	1.293(5)	1.2890(14)	1.295(3)	1.354(1)
C(2)-O(2)	1.351(5)	1.3544(14)	1.356(2)	1.348(1)
i/ii[b]	8.1	4.3	2.9, 3.5	0
iii/iv	6.2	6.8	5.9, 2.5	
v/vi	4.5	3.1	13.7, 9.1	

[a] Bond distances averaged between two independent molecules.

[b] Ring notation is shown in Fig. 4.

Theoretical calculations

Electronic structure calculations were performed on complexes **2**, **4** and **6** to elucidate the nature of the transitions involved in the excitation spectra. The full geometries were optimized at the B3LYP/LANL2DZ:6-31G* level and are denoted **2'**, **4'** and **6'** to distinguish them from experimental data. To assist in assigning the nature of the excited states involved in the experimental absorption spectra, the singlet excited states were obtained based on TD-DFT calculations. The frontier molecular orbitals of **2'**, **4'** and **6'** are shown in Figures S1, 5 and S2 respectively, while the transition character, orbital distributions and the simulated UV-Vis absorption spectra of the complexes, are summarized in Table 3. The computed orbital energies and energy gaps for **2'**, **4'** and **6'** show good agreement with the observed oxidation potentials and trends in photoluminescence measurements (Table 1). All three complexes display similar frontier orbital distributions, with the LUMOs localized mostly on the phenylpyridine based ligands, while the HOMOs are spread across the iridium atom, and the phenoxylate ring of the ancillary ligand. It is noted that the HOMO of **4'** also has a significant contribution from the phenyl rings of the ppy ligands.

Electrophosphorescent device properties

PhOLED devices of complexes **2**, **3**, **5** and **6** were fabricated in the following configuration: ITO/NPB (40 nm)/CBP:**Ir complex**(8%) (30 nm)/TPBi (25 nm)/LiF/Al. All the devices were fabricated by thermal evaporation onto a cleaned glass substrate pre-coated with conductive transparent indium tin oxide (ITO), where 4,4'-bis(*N*-(1-naphthyl)-*N*-phenylamino)biphenyl (NPB) served as a hole-transporting layer (HTL) and 1,3,5-tris(*N*-phenylbenzimidazol-2-yl)benzene (TPBi) as an electron-transporting layer (ETL) and

Table 3. TD-DFT calculation results for complexes **2'**, **4'** and **6'**.

Complex	Transition energy[a]	Participating MO	Transition character[b]	Energy gap / eV
2'	452.3 nm	HOMO→LUMO (96.8%)	L_CL_ACT+ ML_ACT	3.35
	439.3 nm	HOMO→LUMO+1 (98.2%)	L_CL_BCT+ML_BCT+L_CL_ACT	
	376.0 nm	HOMO→LUMO+2 (93.2%)	L_CL_ACT+L_CL_BCT+ML_ACT+ML_BCT	
4'	441.4 nm	HOMO→LUMO (94.9%)	L_CL_BCT+ ML_BCT+ L_AL_BCT	3.55
	409.9 nm	HOMO-1→LUMO (89.4%)	L_CL_BCT+ ML_BCT	
	382.1 nm	HOMO→LUMO+2 (97.2%)	L_BL_CCT+ML_CCT+L_AL_CCT	
6'	421.07 nm	HOMO→LUMO (81.6%) HOMO-1→LUMO (15.3%)	L_CL_BCT+ ML_BCT L_CL_BCT+ ML_BCT+L_AL_BCT	3.62
	404.25 nm	HOMO-1→LUMO (75.2%) HOMO→LUMO (12.8%)	L_CL_BCT+ ML_BCT+L_AL_BCT L_CL_BCT+ ML_BCT	
	355.87 nm	HOMO→LUMO+2 (93.2%)	ML_CCT +L_BL_CCT	

[a] Excitation energies calculated for the excited states. [b] Ligand notation: A, B =2-(2,4-difluorophenyl)pyridyl/2-phenylpyridyl; C =2 -(2'-oxyphenyl)-2-oxazoline/4-(methylsulfonyl)-2-(oxazol-2-yl)phenol

CBP (4,4'-bis(*N*-carbazolyl)-1,1'-biphenyl) is the host. The device structure and the corresponding energy level diagram of the respective active layers are shown in Figure 6a. Complex **4** could not be sublimed, and so devices were not fabricated. The normalized electroluminescence (EL) spectra of the devices at 1000 cd m^{-2} (Figure 6b) are consistent with the photoluminescence (PL) spectra. The EL spectrum of each device

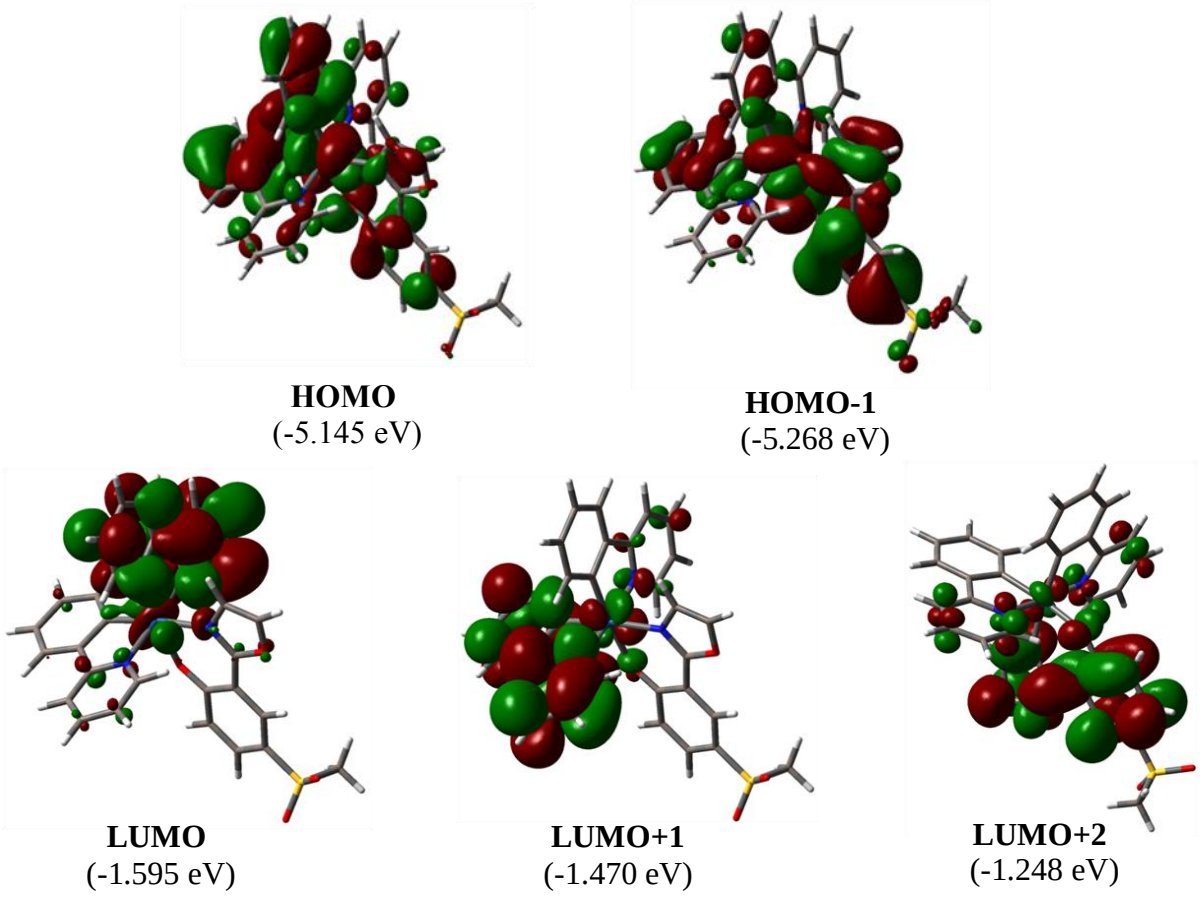

Figure 5. The contour plots of the HOMOs and LUMOs of complex **4'**.

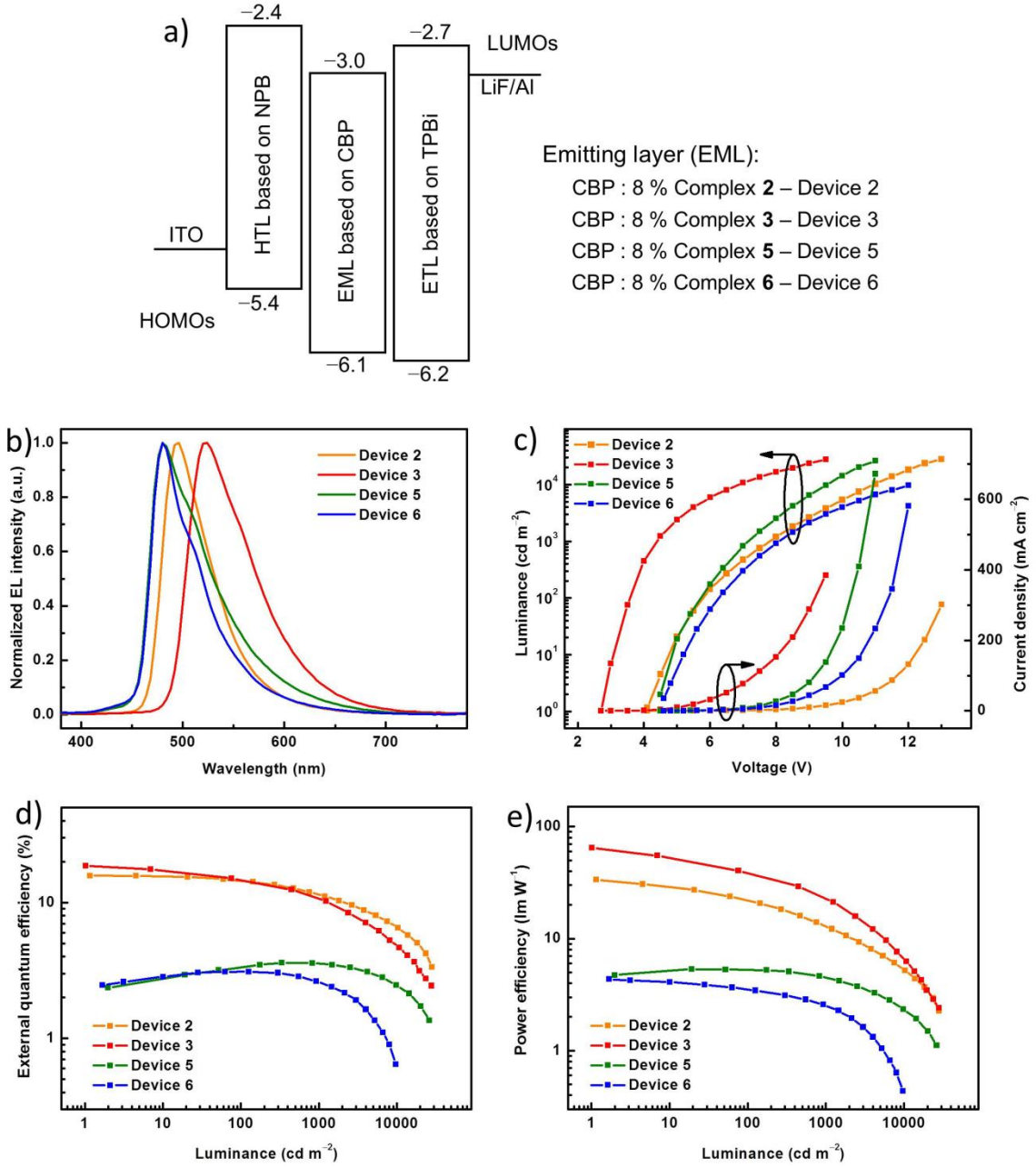

Figure 6. a) Energy diagram of the devices. b) EL spectra of devices at a brightness of 1000 cd m^{-2}. c) Current density-luminance-driving voltage curves of devices. d) EQE-luminance curves of devices. e) PE-luminance curves of devices.

did not change substantially in the whole range of driving voltages, and no host emission was observed in the EL spectra, indicating good exciton confinement on the emissive molecules. Devices 2 and 3 showed the brightest emission in the greenish-blue (λ_{max}^{EL} 496 nm) and green (λ_{max}^{EL} 524 nm) regions, respectively. This result indicates that introducing electron-withdrawing groups such as fluorine onto the cyclometalated (*C^N*) ligand indeed leads to the larger bandgap and the blue shifted emission. Furthermore, complexes **5** and **6** which have the same *C^N* ligand as **2**, exhibited sky-blue emission (λ_{max}^{EL} 480 nm) in the corresponding devices, indicating that the color of electroluminescence could be tuned also through rational structural variations of the ancillary ligands. Here, it is worth noting that the CIE coordinates of devices 5 (0.22, 0.42) and 6 (0.17, 0.38) are very different from each other due to the relatively narrow full spectral width at half maximum (FWHM) of device 6 (Figure 6b), although they possess the same emission peak at λ_{max} 480 nm. These data show that the device emission color can be optimized through adjusting the emission bandwidth,[14] which here has been realized by introducing the different substituents (SO_2Me or CF_3) in the ancillary ligand.

Figures 6c-e show the current density-voltage-luminance, external quantum efficiency and power efficiency-luminance

Table 4: Summary of device data.

Device/ complex	Maximum Brightness / cd m^{-2}	Turn-on voltage[a] / V	EQE[b] / %	PE[b] / lm/W	λ_{ELmax} [c] / nm	$CIE_{x,y}$ [c]
1[d]	61560	3.5	17.7, 17.1, 14.2	47.2, 35.1, 20.8	530	(0.35, 0.61)
2	28130	4.1	15.6, 14.5 11.3	28.5, 21.6, 12.7	496	(0.19, 0.53)
3	28050	2.7	17.3, 14.8, 11.3	52.5, 37.2, 25.5	524	(0.33, 0.61)
5	26150	4.5	2.6, 3.3, 3.5	5.1, 5.3, 4.5	480	(0.22, 0.42)
6	9670	4.6	2.8, 3.1, 2.6	4.1, 3.5, 2.5	480	(0.17, 0.38)

[a] Measured at the brightness of 1 cd m^{-2}. [b] Values at the brightness of 10, 100 and 1000 cd m^{-2} respectively. [c] Values at a brightness of 1000 cd m^{-2}. [d] data taken from ref. 14.

characteristics of the devices 2, 3, 5 and 6. All the devices exhibited a low turn-on voltage (recorded at 1 cd m^{-2}) and the EL intensity rises rapidly after the onset voltages. The corresponding maximum luminance values were obtained at rather low voltages as listed in Table 4. Device 3 exhibited comparable EL efficiency, with the reference device 1 based on the similar green emission,[14] while the other devices exhibited higher driving voltages and lower EL efficiencies attributed to the blue shift in emission compared with devices 1 and 3. This is consistent with the known trend of reduced efficiency upon blue-shifting the emission in this spectral region.[27] These devices generally realized high efficiencies and insignificant efficiency roll-off. Both the EQE and PE values of these devices maintained high levels at luminance values of 10, 100 and 1,000 cd m^{-2}. Such stable and high EL performance based on the simple device structure suggests that the effective charge transport and recombination exists throughout these devices. Notably, devices 2, 3 and 5 reached maximum brightnesses of >26000 cd m^{-2}.

CONCLUSIONS

The new complexes **2-6** have been rationally designed and synthesized, and their optoelectronic and structural properties have been characterized, along with their applications as emitters in PhOLEDs. The emission color of photoluminescence and electroluminescence has been tuned via systematic functionalization of both the cyclometalating ligand and the ancillary ligand, which contribute significantly to the frontier orbital distributions. Exchanging the phenylpyridine (ppy) ligand for 2,4-difluoro-ppy gives a blue shift of 21-22 nm (from **1** to **2**, and from **4** to **5**) and the introduction of electron-withdrawing substituents (SO_2Me, CF_3) onto the phenoxylate ring of the (2´-oxyphenyl)-2-oxazole ligand results in a further blue shift of 13-20 nm. Combining these functionalizations gives λ_{max}^{PL} 476 and 479 for complexes **5** and **6** in dichloromethane solution with PLQYs of ca 0.7. (TD-)DFT calculations are in excellent agreement with the observed photophysical and electrochemical properties of the complexes. PhOLEDs fabricated from the complexes generally demonstrated high efficiencies and very limited efficiency roll-off. Both the EQE and PE values maintained high levels at luminance values of 10, 100 and 1000 cd m^{-2}, with devices 2, 3 and 5 achieving maximum brightnesses of >26000 cd m^{-2}.

Our rational molecular design strategy for tuning the emission color has exploited the unusual frontier orbital distribution in these complexes, namely a significant HOMO character on the phenoxylate part of the ancillary ligand. Functionalization of an ancillary ligand, as developed in this work, is an attractive complementary approach to the more usual methodology of design and synthesis of different (C^N) cyclometalating ligands, where complex formation can be synthetically more challenging for steric and electronic reasons.

EXPERIMENTAL DATA

General procedures

All commercially available chemicals were used without further purification. Reactions requiring an inert atmosphere were performed under a blanket of argon gas, which was dried over a phosphorus pentoxide column. Anhydrous solvents were dried through an HPLC column on an Innovative Technology Inc. solvent purification system. Column chromatography was performed using 40-60 μm mesh silica gel. Analytical TLC was performed on plates pre-coated with silica gel (Merck, silica gel $60F_{254}$) and visualized using UV light (254, 315, 365 nm). NMR spectra were recorded on Bruker Avance 400 MHz, Varian Mercury 200, and 400 MHz, Varian Inova 500 MHz or Varian VNMRS 600 and 700 MHz spectrometers. Chemical shifts are referenced to tetramethylsilane [TMS, $Si(CH_3)_4$] at 0.00 ppm. Melting points were determined in open ended capillaries using a Stuart Scientific SMP3 melting point apparatus at a ramping rate of 1 ^oC/min. They are recorded to the nearest 0.1 ^oC. ESI and MALDI mass spectra were recorded on a Thermo-Finnigan LTQ FT (7.0 T magnet) spectrometer. ASAP mass spectra were recorded on a Waters Xevo QTOF spectrometer. GCMS spectra were recorded on a Thermo-Finnigan Trace GCMS (EI and CI ion sources). Elemental analyses were obtained on an Exeter Analytical Inc. CE-440 elemental analyzer. Microwave reactions were conducted in a sealed vessel in a Biotage Initiator microwave synthesizer (0-400 W). Where solvent mixtures are mentioned any percentage/ratio is by volume.

Electrochemistry

Cyclic voltammetry (CV) data were obtained using a BAS CV50W electrochemical analyzer fitted with a three-electrode system consisting of a Pt disk (Ø = 1.8 mm) as the working electrode, a Pt wire as an auxiliary electrode and an additional platinum wire as the reference electrode. The experiments were conducted in dry DCM solution with $^nBu_4NPF_6$ (0.1 M) as the supporting electrolyte at a scan rate of 100 mV/s. The data were internally referenced to decamethylferrocene, which was then referenced to Fc/Fc^+ to allow comparison with the literature and estimation of the HOMO levels.

Solution photophysics

Solution state photophysical data were obtained using freshly prepared solutions of the complexes in the solvent specified. Emission and lifetime measurements were taken using thoroughly degassed solutions achieved by three freeze−pump−thaw cycles, and obtained using a quartz cuvette with a path length of 1 cm. The solutions had absorbance below 0.10 to minimize inner filter effects. All UV-vis

absorption measurements were recorded using a Unicam UV2-100 spectrometer operated with the Unicam Vision(ver. 3.50) software. Baseline correction was achieved by reference to pure solvent in the same cuvette. Absorption measurements were obtained using quartz cuvettes with a path length of 2 cm. Solution PLQYs were recorded in degassed solvent, and determined using the relative method, with quinine sulfate (Φ_{PL} = 0.546 in 0.5 M H_2SO_4) as the reference. The PLQYs were computed according to the following equation:

$$\Phi_x = \Phi_{ref}\frac{Grad_x}{Grad_{ref}}.\left(\frac{\eta_x}{\eta_{ref}}\right)^2$$

where subscripts 'x' and 'ref' denote the material being measured and the reference, respectively. Φ represents the PLQY, Grad is the gradient of the gradient from the plot of integrated fluorescence intensity vs absorbance, and η is the refractive index of the solvent. Excitation and emission photoluminescence spectra were recorded on a Horiba Jobin Yvon SPEX Fluorolog 3-22 spectrofluorometer. Quantum yields were determined in degassed DCM in comparison with a standard [quinine sulfate = 0.546 in 0.5 M H_2SO_4]. Solutions of the complexes in degassed DCM [$<10^{-5}$ M] were used for decay measurements. The sample was excited by the output of a pulse laser diode which produced a 1 kHz train of pulses of 20 ns duration at 405 nm. The luminescence was collected at 90° and focused onto the entrance slit of a monochromator (Bethan TM 300V). The emission was detected by a photon counting photomultiplier tube and the arrival times of photons at the detector were determined using a multichannel scaler.

X-ray crystallography

X-ray diffraction experiments for **4** and **6** were carried out on a Bruker 3-circle CCD diffractometer D8 Venture with a PHOTON 100 CMOS area detector, using Mo-*K*α radiation from a IμS microsource with focussing mirrors and a Cryostream (Oxford Cryosystems) open-flow N_2 gas cryostat. For **2**, the experiment was carried out at room temperature on a Bruker Smart Apex II CCD diffractometer, using Mo-*K*α radiation (λ = 0.71069 Å). Structure **4** was solved by Patterson methods, **6** by direct methods using SHELXS 2013/1 software[28] and **2** by direct methods using SIR2002 software.[29] The structures were refined in anisotropic approximation by full matrix least squares against F^2 off all data, using OLEX2[30] and SHELXL 2014/7 software.[31] The asymmetric unit of **4** contains one complex molecule and two molecules of THF, one of them partly disordered. The asymmetric unit of **6** contains two complex molecules (both with rotationally disordered CF_3 groups) and one disordered solvent molecule. Presumably, the latter site is shared by DCM and $CDCl_3$ molecules in a 0.8:0.2 ratio. The asymmetric unit of **2** contains one complex molecule and half of one DCM molecule, the latter having crystallographic C_2 symmetry.

Thermal Analysis

Thermogravimetric analysis (TGA) was performed in a nitrogen atmosphere using a Perkin-Elmer Pyris 1 TGA instrument. The complexes were heated at a rate of 10 °C /min from room temperature up to 600 °C.

Synthesis and Characterization

Iridium complex 2

$IrCl_3.3H_2O$ (209 mg, 0.59 mmol) was added to a stirred solution of 2-(2,4-difluorophenyl)pyridine (250 mg, 1.31 mmol) in 2-ethoxyethanol (6 mL) under argon. The solution was heated to 135 °C for 6 h, before 2-(2'-hydroxyphenyl)-2-oxazoline **21**[14,19] (121 mg, 0.74 mmol) and Na_2CO_3 (315 mg, 2.97 mmol) were added and the solution was heated at 135 °C overnight. Water was added and the yellow precipitate was collected by filtration. The residue was purified by column chromatography (hexane:EtOAc 4:1) to give complex **2** as a yellow solid (310 mg, 79%); Anal. Calc. for $C_{31}H_{20}F_4IrN_3O_2$: C, 50.68; H, 2.74; N, 5.72. Found: C, 50.43; H, 3.07; N, 5.47; δ_H (400 MHz; CD_2Cl_2) 8.78 (1H, d, *J* 5.2), 8.39 (1H, d, *J* 5.8), 8.26 (2H, t, *J* 8.9), 7.87 – 7.75 (2H, m), 7.61 (1H, d, *J* 8.1), 7.21 (1H, t, *J* 6.6), 7.14 (2H, t, *J* 7.0), 6.60 (1H, d, *J* 8.7), 6.45 – 6.32 (3H, m), 5.79 (1H, dd, *J* 8.9, 2.3), 5.62 (1H, dd, *J* 8.9, 2.4), 4.36 (1H, q, *J* 9.3), 4.23 (1H, q, *J* 8.5), 3.64 – 3.47 (1H, m), 3.14 – 3.00 (1H, m); δ_F (376 MHz CD_2Cl_2;) -109.30 (1F, q, *J* 9.1), -109.34 (1F, q, *J* 9.3), -110.90 (1F, ddd, *J* 12.4, 10.1, 1.6), -110.95 (1F, ddd, *J* 12.5, 10.1, 2.5); HRMS (FTMS+ESI): calcd for $[C_{31}H_{20}F_4N_3O_2Ir+H]+$: 734.1176. Found: 734.1186. Crystals for X-ray analysis were grown by slow evaporation of a DCM/methanol solution of **2**.

***N*-(2,2-diethoxyethyl)-2-methoxybenzamide 8**

Methyl-2-methoxybenzoate **7** (5.00 g, 28.93 mmol) and aminoacetaldehyde diethylacetal (2.78 g, 17.25 mmol) were combined and the mixture was heated to 160 °C for 4 h before being cooled to RT. An NMR spectrum of the crude material showed the reaction had not gone to completion; more aminoacetaldehyde diethylacetal (1.00 g, 6.20 mmol) was added and the reaction was heated to 160 °C overnight before being cooled to RT. Any methanol produced was removed by rotary evaporation and the oily residue was purified by column chromatography (hexane:EtOAc 1:1) to give an oil, *N*-(2,2-diethoxyethyl)-2-methoxybenzamide **8** (2.80 g, 36%); δ_H (400 MHz; $CDCl_3$) 8.21 (1H, dd, *J* 7.8, 1.9), 8.15 (1H, br t, *J* 5.5), 7.45 (1H, ddd, *J* 8.3, 7.3, 1.8), 7.08 (1H, ddd, *J* 7.8, 7.3 1.0), 6.98 (1H, dd, *J* 8.4, 1.0), 4.63 (1H, t, *J* 5.6), 3.97 (3H, s), 3.76 (dq, *J* 9.4, 7.0), 3.67 – 3.54 (4H, m), 1.25 (6H, t, *J* 7.0); HRMS (FTMS+ESI): calcd for $[C_{14}H_{21}NO_4+Na]+$: 290.1368. Found: 290.1368. The ^{13}C NMR spectrum could not be obtained as **8** hydrolyzed to the aldehyde in the NMR solvent; δ_H (600 MHz; $CDCl_3$) 9.76 (1H, d, *J* 0.6), 8.64 (1H, br s), 8.21 (1H, dd, *J* 7.7, 1.9), 7.51 – 7.45 (1H, m), 7.09 (1H, t, *J* 7.6), 7.01 (1H, d, *J* 8.4), 4.41 (2H, dd, *J* 4.8, 0.7), 4.03 (3H, d, *J* 0.6); δ_C (151 MHz; $CDCl_3$) 196.97, 165.69, 157.96, 133.45, 132.52, 121.48, 120.70, 111.55, 56.20, 51.15.

2-(2-methoxyphenyl)oxazole 9 and 2-(2-methoxy-5-(methylsulfonyl)phenyl)oxazole 10

Methanesulfonic acid (35 mL) was added cautiously to *N*-(2,2-diethoxyethyl)-2-methoxybenzamide **8** (2.80 g, 11.70 mmol) with stirring. P_4O_{10} (4.50 g, 15.85 mmol) was added with caution and the mixture was heated to 180 °C overnight. The mixture was cooled to RT and added dropwise to aq. $NaHCO_3$ solution (300 mL) with stirring. The aqueous phase (pH 8) was extracted with DCM (3 × 400 mL) and the solvent was removed *in vacuo* to leave a thick oil. The residue was purified by column chromatography (10-20% EtOAc in DCM) to give the product **9** as a yellow oil (400 mg, 19%); δ_H (400 MHz; $CDCl_3$) 7.98 (1H, dd, *J* 8.1, 1.8), 7.76 (1H, d, *J* 0.8), 7.46 (1H, ddd, *J* 8.3, 7.4, 1.8), 7.31 (1H, d, *J* 0.8), 7.04- 7.11 (2H, m), 4.00 (3H, s); δ_C (151 MHz; $CDCl_3$) 160.44, 157.67, 138.31, 131.90, 130.41, 128.28, 120.79, 116.61, 112.10, 56.20; HRMS (FTMS+ESI): calcd for $[C_{10}H_9NO_2+H]^+$: 176.0712. Found: 176.0740.

Also isolated was a second fraction: 2-(2-methoxy-5-(methylsulfonyl)phenyl)oxazole **10** (538 mg, 18%); δ_H (400 MHz; $CDCl_3$) 8.54 (1H, dd, *J* 2.4, 0.8), 8.01 (1H, ddd, *J* 8.8, 2.4, 0.8), 7.78 (1H, d, *J* 0.8), 7.33 (1H, s), 7.18 (1H, d, *J* 8.8), 4.07 (3H, s), 3.09 (3H, s); δ_C (151 MHz; $CDCl_3$) 161.29, 158.31*, 139.10, 131.21, 130.18, 128.69, 117.36*, 112.49, 56.85, 44.94, (* denotes carbons identified from the HMBC spectrum). One carbon is not observed due to low solubility; HRMS (FTMS+ESI): calcd for $[C_{11}H_{11}NO_4S+H]^+$: 254.0487. Found: 254.0471.

2-(oxazol-2-yl)phenol 11

BBr_3 (0.65 ml, 6.87 mmol) was added dropwise to a stirred solution of 2-(2-methoxyphenyl)oxazole **9** (400 mg, 2.28 mmol) in DCM (10 mL, dry) over an ice bath. The suspension was stirred at RT overnight before the reaction was quenched with water (CAUTION). The solid formed, presumed to be (2-(2-hydroxyphenyl)oxazol-3-ium bromide) was filtered off and suspended in DCM. This was then washed with aq. Na_2CO_3 to neutralize the salt. The organic phase was collected and the aqueous phase was washed with further DCM (3 × 50 mL). The organic phases were combined, dried over $MgSO_4$ and filtered. The solvent was removed *in vacuo* to give an oil, 2-(oxazol-2-yl)phenol **11** (250 mg, 68%); δ_H (700 MHz; $CDCl_3$) 11.20 (1H, s), 7.84 (1H, dd, *J* 7.8, 1.7), 7.69 (1H, t, *J* 0.9), 7.39 – 7.34 (1H, m), 7.24 (1H, d, *J* 1.0), 7.08 (1H, dd, *J* 8.3, 1.2), 6.95 (1H, td, *J* 7.5, 1.0); δ_C (176 MHz; $CDCl_3$) 161.78, 157.35, 137.49, 132.47, 126.51, 126.08, 119.52,

117.31, 111.25; HRMS (FTMS+ESI): calcd for $[C_9H_7NO_2+H]^+$: 162.0555. Found: 162.0542.

4-(methylsulfonyl)-2-(oxazol-2-yl)phenol 12

BBr_3 (0.61 mL, 6.37 mmol) was added dropwise to a stirred solution of 2-(2-methoxy-5-(methylsulfonyl)phenyl)oxazole **10** (538 mg, mmol) in DCM (10 mL, dry) over an ice bath. The suspension was stirred at RT overnight before the reaction was quenched with water (CAUTION). The solid formed, presumed to be 2-(2-hydroxy-5-(methylsulfonyl)phenyl)oxazol-3-ium bromide, was filtered off and suspended in DCM. This was then washed with aq. Na_2CO_3 to neutralize the salt. The organic phase was collected and the aqueous phase was washed with further DCM (3 × 50 mL). The organic phases were combined, dried over $MgSO_4$ and filtered. TLC revealed a mixture of starting material and product; the crude mixture was redissolved in DCM and extracted with aq. NaOH solution (3 × 50 mL, 1 M). The aqueous phases were combined, acidified to pH 6 with conc. HCl and re-extracted with DCM (4 × 100 mL). The organic phase was dried over $MgSO_4$, the solvent was removed and the residue was purified by silica plug (EtOAc) to give a white solid, 4-(methylsulfonyl)-2-(oxazol-2-yl)phenol **12** (200 mg, 39%) which was recrystallized from methanol. δ_H (400 MHz; $CDCl_3$) 11.91 (1H, s), 8.47 (1H, d, *J* 2.4), 7.91 (1H, dd, *J* 8.8, 2.4), 7.79 (1H, d, *J* 0.9), 7.32 (1H, d, *J* 0.9), 7.23 (1H, d, 8.8), 3.10 (3H, s); δ_C (101 MHz; $CDCl_3$) 161.39, 160.21, 138.54, 131.68, 131.30, 126.78, 126.56, 118.56, 111.65, 45.01; HRMS (FTMS+ESI): calcd for $[C_{10}H_9NO_4S]^+$: 240.0331. Found: 240.0335.

Iridium complex 3

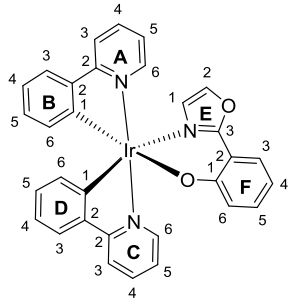

$IrCl_3.3H_2O$ (123 mg, 0.35 mmol) was added to a stirred solution of 2-phenylpyridine (0.11 mL, 0.77 mmol) in 2-ethoxyethanol (10 mL). The solution was heated to reflux (135 ^oC) overnight. Na_2CO_3 (300 mg, 2.83 mmol) and 2-(oxazol-2-yl)phenol **11** (62 mg, 0.38 mmol) were added and the solution was heated to reflux overnight before being cooled to RT. Water was added and the precipitate was filtered to give a yellow solid. The crude product was filtered and washed with more water to remove water-soluble impurities. The product was dried, then washed with hexane and cold diethyl ether to remove traces of ppy ligand. The product was obtained as a yellow solid, **3** (200 mg, 87%); Anal. Calc. for $C_{31}H_{22}IrN_3O_2.0.25CH_2Cl_2$: C, 55.00; H, 3.33; N, 6.17. Found: C, 55.18; H, 3.26; N, 6.02; δ_H (700 MHz; $CDCl_3$) 8.88 (1H, d, *J* 5.7, H_{A6}), 7.99 (1H, d, *J* 5.8, H_{C6}), 7.85 (1H, d, *J* 8.2, H_{C3}), 7.80 (1H, d, *J* 8.2, H_{A3}), 7.72 (1H, dd, *J* 8.2, 1.9, H_{F3}), 7.67 (1H, td, *J* 8.1, 1.5, H_{A4}), 7.65 (1H, td, *J* 8.1, 1.5, H_{C4}), 7.59 (1H, dd, *J* 7.9, 1.1, H_{D3}), 7.56 (1H, dd, *J* 7.6, 1.1, H_{B3}), 7.38 (1H, d, *J* 1.0, H_{E2}), 7.12 (1H, ddd, *J* 8.7, 7.0, 1.9, H_{F5}), 7.07 (1H, ddd, *J* 7.4, 6.0, 1.4, H_{A5}), 6.92 (1H, ddd, *J* 8.1, 5.9, 1.4, H_{C5}), 6.87 (1H, td, *J* 7.5, 1.2, H_{D4}), 6.86 (1H, td, *J* 7.4, 1.2, H_{B4}), 6.80 – 6.75 (2H, m, H_{F6+D5}), 6.73 (1H, dt, *J* 7.3, 1.1, H_{B5}), 6.42 (1H, ddd, *J* 7.9, 6.9, 1.1, H_{F4}), 6.36 (1H, d, *J* 7.6, H_{B6}), 6.28 (1H, d, *J* 7.6, H_{D6}), 6.20 (1H, d, *J* 1.0, H_{E1}); δ_C (151 MHz; $CDCl_3$) 169.22 (C_{C2}), 168.10 (C_{A2}), 167.20 (C_{F1}), 158.67 (C_{E3}), 152.67 (C_{D1}), 149.07 (C_{A6}) 148. 72 (C_{B1}), 148.67 (C_{C6}), 144.87 (C_{B2}), 144.83 (C_{D2}), 137.49 (C_{E2}), 136.91 (C_{A4}), 136.74 (C_{C4}), 133.20 (C_{B6}), 132.56 (C_{F5}), 132.48 (C_{D6}), 129.69 (C_{B5}), 129.58 (C_{D5}), 127.39 (C_{F3}), 126.64 (C_{E1}), 125.53 (C_{F6}), 124.18 (C_{B3}), 124.10 (C_{D3}), 122.07 (C_{A5}) 121.80 (C_{C5}), 120.79 (C_{D4}), 119.02 (C_{B4}), 118.73 (C_{C3}), 118.25 (C_{A3}), 113.34 (C_{F4}), 110.94 (C_{F2}); HRMS (FTMS+ESI): calcd for $[C_{31}H_{22}N_3O_4{}^{191}Ir+H]^+$: 660.1396. Found: 660.1406.

Iridium complex 4

$IrCl_3.3H_2O$ (236 mg, 0.67 mmol) was added to a stirred solution of 2-phenylpyridine (0.21 mL, 1.47 mmol) in 2-ethoxyethanol (10 mL). The solution was heated to reflux (135 ^oC) overnight. Na_2CO_3 (354 mg, 3.34 mmol) and 4-(methylsulfonyl)-2-(oxazol-2-yl)phenol **12** (200 mg, 0.84 mmol) were added and the solution was heated to reflux overnight before being cooled to RT. Water was added and the precipitate was filtered to give a yellow solid. The crude material was purified by column chromatography (10% EtOAc in DCM) to give the product as a yellow solid. Fractions containing product **4** contaminated with unreacted ppy were combined, the solvent was then removed and the solid was washed with hexane to give additional product **4** (combined yield: 281 mg, 57%); Anal. Calc. for $C_{32}H_{24}IrN_3O_4S$: C, 52.02; H, 3.27; N, 5.69. Found: C, 51.84; H, 3.61; N, 5.27; δ_H (400 MHz; $CDCl_3$) 8.75 (1H, ddd, *J* 5.8, 1.5, 0.7), 8.38 (1H, d, *J* 2.6), 7.96 (1H, d, *J* 5.7, 1.5, 0.7), 7.91 (1H, d, *J* 8.1), 7.87 (1H, d, *J* 8.1), 7.75 (1H, td, *J* 7.6, 1.7), 7.73 (1H, td, *J* 7.5, 1.6), 7.60 (1H, td, *J* 8.4, 1.1), 7.57 (1H, dd, *J* 9.2, 2.6), 7.49 (1H, d, *J* 1.0), 7.14 (1H, ddd, *J* 7.3, 5.7, 1.4), 7.01 (1H, ddd, *J* 7.4, 5.8, 1.5), 6.93 (1H, td, *J* 7.5, 1.2), 6.92 (1H, td, *J* 7.5, 1.2), 6.82 (1H, d, *J* 9.2), 6.79 (1H, td, *J* 6.16, 1.2), 6.76 (1H, td, *J* 7.4, 1.4), 6.83 – 6.77 (1H, m), 6.79 – 6.74 (m, 1H), 6.38 (1H, dd, *J* 7.7, 1.0), 6.29 (1H, dd, *J* 7.6, 1.0), 6.27 (1H, d, *J* 1.0), 3.04 (s, 3H); HRMS (FTMS+ESI): calcd for $[C_{32}H_{24}N_3O_4S^{191}Ir]^+$: 737.1094. Found: 737.1118. Crystals for X-ray analysis were grown by slow evaporation of a solution of **4** in tetrahydrofuran.

***N*-(2,2-diethoxyethyl)-2-methoxy-5-(methylsulfonyl)-benzamide 15**

$SOCl_2$ (15 mL) was added to 2-methoxy-5-(methylsulfonyl)benzoic acid **13** (6.00 g, 26.06 mmol) and the mixture was heated to reflux under a nitrogen atmosphere for 3 h, before being cooled to RT. The excess $SOCl_2$ was removed *in vacuo* to leave an off-white solid, 2-methoxy-5-(methylsulfonyl)benzoyl chloride, which was used without further purification. A solution of 2-methoxy-5-(methylsulfonyl)benzoyl chloride in DCM (20 mL) was added dropwise to a stirred solution of aminoacetaldehyde diethylacetal (4.16 mL, 28.66 mmol), NEt_3 (0.33 mL, 28.66 mmol) in DCM (40 mL). The reaction was left to stir at RT overnight. The solvent was removed *in vacuo*, and solid was then suspended in water and sonicated, followed by stirring. The product was then collected via filtration. This washing was repeated a second time, and the product was collected as a white solid, *N*-(2,2-diethoxyethyl)-2-methoxy-5-(methylsulfonyl)-benzamide **15** (7.25 g, 81%); δ_H (400 MHz; $CDCl_3$) 8.77 (1H, d, *J* 2.6), 8.04 (1H, dd, *J* 8.7, 2.6), 7.94 (1H, s), 7.13 (1H, d, *J* 8.8), 4.63 (1H, t, *J* 5.4), 4.07 (3H, s), 3.76 (2H, dq, *J* 9.4, 7.1), 3.67 – 3.53 (4H, m), 3.06 (3H, s), 1.25 (6H, t, *J* 7.0); δ_C (101 MHz; $CDCl_3$) 163.49, 161.14, 133.64, 132.39, 132.09, 122.90, 112.13, 100.86, 63.02, 56.77, 44.66, 42.60, 15.53; the molecular ion was not observed and the product was characterized by fragment ions, MS (ASAP+): $[M\text{-}OEt]^+$ = 300.1 $[M\text{-}NHCH_2CH(OEt)_2]^+$ = 213.0.

***N*-(2,2-diethoxyethyl)-2-methoxy-5-trifluoromethyl-benzamide 16**

$SOCl_2$ (7 mL) was added to 2-methoxy-5-(trifluoromethyl)benzoic acid **14** (1.37 g, 6.22 mmol) and the mixture was heated to reflux under a nitrogen atmosphere for 3 h, before being cooled to RT. The excess $SOCl_2$ was removed *in vacuo* to leave an off-white solid, 2-methoxy-5-trifluoromethylbenzoyl chloride, which was used without further purification. A solution of 2-methoxy-5-trifluoromethylbenzoyl chloride in DCM (5 mL) was added dropwise to a stirred solution of aminoacetaldehyde diethylacetal (1.00 mL, 6.84 mmol), NEt_3 (0.95 ml, 6.84 mmol) in DCM (20 mL). The reaction was stirred at RT overnight, before the solvent was removed *in vacuo*. The resulting solid was then suspended in water and sonicated, followed by stirring. The product was then collected via filtration. This was repeated a second time, and the product was collected as a white solid, *N*-(2,2-diethoxyethyl)-2-methoxy-5-trifluoromethyl-benzamide **16** (2.00 g, 97%); δ_H (400 MHz; $CDCl_3$) 8.51 (1H, d, *J* 2.5), 8.04 (1H, br s), 7.70 (1H, ddd, *J* 8.7, 2.6, 0.8), 7.07 (1H, d, *J* 8.7), 4.63 (1H, t, *J* 5.4), 4.03 (3H, s), 3.76 (2H, dq, *J* 9.4, 7.0), 3.67 – 3.53 (4H, m), 1.25 (6H, t, *J* 7.0); δ_F (376 MHz; $CDCl_3$) -61.89 (3F, d, *J* 0.8); δ_C (101 MHz; $CDCl_3$) 164.06, 159.77, 130.16 (q, *J* 3.8), 129.83 (q, *J* 3.8), 124.08 (q, *J* 272.1), 123.96 (q, *J* 32.3), 122.10, 111.76, 100.99, 63.01, 56.48, 42.58, 15.54; HRMS (FTMS+ESI): calcd for $[C_{15}H_{20}F_3NO_4+Na]^+$: 358.1242. Found: 358.1245.

2-methoxy-5-(methylsulfonyl)-*N*-(2-oxoethyl)benzamide 17

Dilute HCl (2 drops, 2 M) was added to a stirred solution of *N*-(2,2-diethoxyethyl)-2-methoxy-5-(methylsulfonyl)-benzamide **15** (2.00 g, 5.79 mmol) in acetone/water (60 mL/20 mL) and the mixture was heated to reflux for 5 h before stirring at RT overnight. The solvent was removed *in vacuo* to give the product, 2-methoxy-5-(methylsulfonyl)-*N*-(2-oxoethyl)benzamide **17** (1.57 g, 100%); δ_H (400 MHz; $CDCl_3$) 9.78 (1H, s), 8.77 (1H, d, *J* 2.5), 8.49 (1H, br s), 8.07 (1H, dd, *J* 8.8, 2.5), 7.17 (1H, d, *J* 8.8), 4.46 (2H, d, *J* 4.7), 4.14 (3H, s), 3.07 (3H, s); δ_C (101 MHz; $CDCl_3$) 196.11, 163.56, 161.37, 133.77, 132.57, 132.53, 122.04, 112.30, 57.00, 51.28, 44.70; HRMS (FTMS+ESI): calcd for $[C_{11}H_{13}NO_5S+H]^+$: 272.0593. Found: 272.0606.

2-methoxy-*N*-(2-oxoethyl)-5-(trifluoromethyl)benzamide 18

HCl (2 drops, 2M) was added to a stirred solution of N-(2,2-diethoxyethyl)-2-methoxy-5-trifluoromethyl-benzamide **16** (2.00 g, 5.96 mmol) in acetone/water (30 mL/10 mL), and the mixture was heated to reflux for 4 h before being stirred at RT overnight. The solvent was removed *in vacuo* to give the product, 2-methoxy-*N*-(2-oxoethyl)-5-(trifluoromethyl)benzamide **18** (1.56 g, 100%.); δ_H (400 MHz; $CDCl_3$) 9.78 (1H, s), 8.57 (1H, br s), 8.51 (1H, d, *J* 2.4), 7.73 (1H, ddd, *J* 8.7, 2.5, 0.8), 7.11 (1H, d, *J* 8.7), 4.45 (2H, d, *J* 4.7), 4.10 (3H, s); δ_F (376 MHz; $CDCl_3$) -61.92 (3F, s); δ_C (176 MHz; $CDCl_3$) 196.3, 164.17, 160.00 (d, *J* 0.9), 130.31 (q, *J* 3.8), 130.21 (q, *J* 3.8), 124.04 (q, *J* 32.1), 124.03 (q, *J* 271.6), 121.23, 111.90, 56.69, 51.25; HRMS (FTMS+ESI): calcd for $[C_{11}H_{10}NO_3F_3+H]^+$: 262.0691. Found: 262.0693

2-(2-methoxy-5-(methylsulfonyl)phenyl)oxazole 10

Burgess' reagent (2.07 g, 8.69 mmol) was added to a solution of 2-methoxy-5-(methylsulfonyl)-*N*-(2-oxoethyl)benzamide **17** (1.57 g, 5.79 mmol) in THF (15 mL) in a 20 mL microwave vial. The reaction was heated to 70 °C in the microwave for 10 min with stirring. Once cooled, the solvent was removed and the residue purified by column chromatography (EtOAc) to give the product, 2-(2-methoxy-5-(methylsulfonyl)phenyl)oxazole **10** (0.30 g, 20%); NMR data were consistent with the sample obtained previously (see above).

Iridium complex 5

$IrCl_3.3H_2O$ (120 mg, 0.34 mmol) was added to a solution of dfppy (143 mg, 0.75 mmol) in 2-ethoxyethanol (5 mL) and the mixture was heated to 130 °C overnight under a nitrogen atmosphere. The mixture was cooled, and Na_2CO_3 (180 mg, 1.70 mmol) and 4-(methylsulfonyl)-2-(oxazol-2-yl)phenol **12** (102 mg, 0.43 mmol) were added. The solution was heated to reflux overnight under a nitrogen atmosphere, before being cooled to RT, and the solvent removed *in vacuo*. The residue was purified by column chromatography (hexane:acetone 2:1). The solid obtained was dissolved in methanol, and triturated with hexane to give the product as a yellow solid (197 mg, 71%); Anal. Calc. for $C_{32}H_{20}IrN_3O_4F_4S$: C, 47.40; H, 2.49; N, 5.18. Found: C, 47.00; H, 2.56; N, 5.07; δ_H (400 MHz; Acetone-d_6) 8.76 (1H, ddd, *J* 5.8, 1.7, 0.8), 8.36 – 8.26 (4H, m), 8.09 – 7.97 (3H, m), 7.56 (1H, dd, *J* 9.1, 2.6), 7.44 (1H, ddd, *J* 7.4, 5.8, 1.4), 7.28 (1H, ddd, *J* 7.4, 5.8, 1.5), 6.68 (1H, d, *J* 9.1), 6.60 (1H, ddd, *J* 12.8, 9.4, 2.4), 6.56 (1H, ddd, *J* 12.8, 9.4, 2.4), 6.46 (1H, d, *J* 1.1), 5.84 (1H, dd, *J* 8.8, 2.4), 5.67 (1H, dd, *J* 8.9, 2.4), 3.03 (3H, s); δ_F (376 MHz; Acetone-d_6) -109.37 (1F, q, *J* 9.4), -110.28 (1F, q, *J* 9.5), -111.32 (1F, t, *J* 11.5), -112.06 (1F, t, *J* 11.3); HRMS (FTMS+ESI): calcd for $[C_{32}H_{20}N_3O_4F_4S^{191}Ir+H]^+$: 810.0795. Found: 810.0803.

2-(2-methoxy-5-(trifluoromethyl)phenyl)oxazole 19

Burgess' reagent (0.43 g, 1.80 mmol) was added to a solution of 2-methoxy-*N*-(2-oxoethyl)-5-(trifluoromethyl)benzamide **18** (0.24 g, 0.92 mmol) in THF (4 mL) in a 2-5 mL microwave vial. Five vials were set up, and the reactions were heated to 70 °C in the microwave for 10 min with stirring. Once cooled, the solutions were combined and the solvent was removed. The residue was purified by column chromatography (initially DCM, changed to 10% EtOAc in DCM) to give the product, 2-(2-methoxy-5-(trifluoromethyl)phenyl)oxazole **19** (440 mg, 40%); δ_H (400 MHz; $CDCl_3$) 8.24 (1H, d, *J* 2.4), 7.77 (1H, d, *J* 0.8), 7.68 (1H, ddd, *J* 8.8, 2.5, 0.8), 7.32 (1H, d, *J* 0.8), 7.12 (1H, d, *J* 8.8), 4.03 (3H, s); δ_F (376 MHz; $CDCl_3$) -61.80 (3F, d, *J* 0.8); δ_C (101 MHz; $CDCl_3$) 159.77, 159.13, 138.85, 128.76 (q, *J* 3.8), 128.62, 127.79 (q, *J* 3.8), 124.11 (q, *J* 271.0), 123.23 (q, *J* 33.1), 117.00, 112.14, 56.54; HRMS (FTMS+ESI): calcd for $[C_{11}H_8NO_2F_3+H]^+$: 244.0585. Found: 244.0580.

4-(trifluoromethyl)-2-(oxazol-2-yl)phenol 20

2-(2-Methoxy-5-(trifluoromethyl)phenyl)oxazole **19** (440 mg, 1.81 mmol) was added to a molten pyridine hydrochloride (8.00 g, 69.22 mmol) at 160 °C. The reaction was heated at 160 °C for 6 h before being cooled to RT. Water (40 mL) and EtOAc (40 mL) were added, and the layers were separated. The organic layer was washed with further water (3 × 50 mL), then dried over $MgSO_4$ and the solvent removed *in vacuo*. The residue was purified by column chromatography (DCM) to give a mixture of the product, 4-(trifluoromethyl)-2-(oxazol-2-yl)phenol **20** and a decomposition product (102 mg). **20**; δ_H (400 MHz; $CDCl_3$) 11.60 (1H, s), 8.15 (1H, d, *J* 2.0), 7.78 (1H, d, *J* 0.9), 7.62 (1H, ddd, *J* 8.7, 2.3, 0.7), 7.32 (1H, d, *J* 0.9), 7.18 (1H, d, *J* 8.6); δ_F (376 MHz; $CDCl_3$) -62.01 (3F, s); HRMS (FTMS+ESI): calcd for $[C_{10}H_6NO_2F_3+H]^+$: 230.0429. Found: 230.0423.

The decomposition product was identified by NMR and mass spectrometry as 2-hydroxy-5-(trifluoromethyl)-benzamide.

Iridium complex 6

$IrCl_3.3H_2O$ (170 mg, 0.41 mmol) was added to a solution of dfppy (170 mg, 0.89 mmol) in 2-ethoxyethanol (5 mL) and the mixture was heated to 130 °C overnight under a nitrogen atmosphere. The mixture was cooled, and Na_2CO_3 (214 mg, 2.02 mmol) and 2-(2-methoxy-5-(trifluoromethyl)phenyl)oxazole **20** (102 mg, 0.45 mmol) were added. The solution was heated to reflux overnight under a nitrogen atmosphere, before being cooled to RT, and the solvent removed *in vacuo*. The residue was purified by column chromatography (hexane:EtOAc 2:1) to give the product as a yellow solid, complex **6** (160 mg, 50%); Anal. Calc. for $C_{32}H_{17}IrN_3O_2F_7$: C, 48.00; H, 2.14; N, 5.25. Found: C, 48.53; H, 2.31; N, 5.18; δ_H (400 MHz; Acetone-d_6) 8.79 (1H, ddd, *J* 5.7, 1.7, 0.8), 8.36 – 8.26 (3 H, m), 8.09 – 7.96 (4H, m), 7.43 (1H, ddd, *J* 7.3, 5.8, 1.4), 7.35 (1H, dd, *J* 9.1, 2.6), 7.27 (1H, ddd, *J* 7.4, 5.8, 1.5), 6.69 (1H, d, *J* 8.9), 6.57 (2H, dddd, *J* 18.7, 12.8, 9.4, 2.4), 6.44 (1H, d, *J* 1.1), 5.85 (1H, dd, *J* 8.8, 2.4), 5.67 (1H, dd, *J* 8.8, 2.4), 2.81 – 2.75 (2H, m), 2.09 (3H, s); δ_F (376 MHz; Acetone-d_6) -61.42 (3F, m), -109.45 (1F, q, *J* 9.4), -110.37 (1F, q, *J* 9.4), -111.38 (1F, t, *J* 11.5), -112.14 (1F, ddd, *J* 12.4, 9.9, 1.7); HRMS (FTMS+ESI): calcd for $[C_{32}H_{17}N_3O_2F_7{}^{191}Ir+H]^+$: 800.0893. Found: 800.0883. Crystals for X-ray analysis were grown by slow evaporation of a DCM/$CDCl_3$/hexane solution of **6** in an NMR tube.

ASSOCIATED CONTENT

Supporting Information

Crystal data have been deposited with the Cambridge Crystallographic database as CCDC numbers 1512945-1592947.

NMR spectra, additional computational, photophysical and electrochemical data, Cartesian coordinates of optimized geometries (PDF) and X-ray crystallographic data (CIF).

AUTHOR INFORMATION

Corresponding Authors

* m.r.bryce@durham.ac.uk; yuliu@jlu.edu.cn; zhudx047@nenu.edu.cn

Notes The authors declare no competing financial interest.

ACKNOWLEDGEMENT. We thank Durham University for a doctoral scholarship (to H.B.), EPSRC grant EP/K039423/1 for funding work in Durham, and NSFC (No. 51373062, 51473028), the key scientific and technological project of Jilin province (20150204011GX, 20160307016GX), the development and reform commission of Jilin province (20160058) in China.

REFERENCES

[1] Yam, V. W.-W.; Wong, K. M.-C. *Chem. Comm.* **2011**, *47*, 11579-11592.
[2] (a) Liu, S.; Zhou, N.; Chen, Z.; Wei, H.; Zhu, Y.; Guo, S.; Zhao, Q. *Opt. Lett.* **2017**, *42*, 13-16. (b) Liu, S.; Zhang, Y.; Liang, H.; Chen, Z.; Liu, Z.; Zhao, Q. *Opt. Express* **2016**, *24*, 15757-15764. (c) Liu, S.; Xu, A.; Chen, Z.; Ma, Y.; Yang, H.; Shi, Z.; Zhao, Q. *Opt. Express* **2016**, *24*, 28247-28255.
[3] Sun, H.; Liu, S.; Lin, W.; Zhang, K. Y.; Lv, W.; Huang, X.; Huo, F.; Yang, H.; Jenkins, G.; Zhao, Q.; Huang, W. *Nat. Commun.* **2014**, *5*, 3601-3610.
[4] (a) Luminescent Complexes and Materials for Light-Emitting Devices: Themed Issue *Dalton Trans.* **2015**, *44*, 8317-8317. (b) Mertens, R., The OLED Handbook. A Guide to OLED Technology, Industry and Market, 2014: www.oled-info.com/handbook. (c) Yang, X.; Zhou, G.; Wong, W.-Y. *Chem. Soc. Rev.* **2015**, *44*, 8484-8575. (d) Xiao, L.; Chen, Z.; Qu, B.; Luo, J.; Kong, S.; Gong, Q.; Kido, J. *Adv. Mater.* **2011**, *23*, 926-952. (e) Cloy, W. C. H.; Chan, W. K.; Yuan, Y. *Adv. Mater*. **2014**, *26*, 5368-5399.
[5] (a) Kamtekar, K. T.; Monkman, A. P.; Bryce, M. R. *Adv. Mater.* **2010**, *22*, 572. (b) Ying, L.; Ho, C.-L.; Wu, H.; Cao, Y.; Wong, W.-Y. *Adv. Mater.* **2014**, *26*, 2459-2473.
[6] (a) Baldo, M. A.; Thompson, M. E.; Forrest, S. R. *Nature* **2000**, *403*, 750-753. (b) Lamansky, S.; Djurovich, P.; Murphy, D.; Abdel-Razzaq, F.; Lee, H.-E.; Adachi, C.; Burrows, P. E.; Forrest, S. R.; Thompson, M. E. *J. Am. Chem. Soc.* **2001**, *123*, 4304-4312.
[7] Chou, P. T.; Chi, Y. *Chem. Eur. J.* **2007**, *13*, 380-395.
[8] (a) Ladouceur, S.; Zysman-Colman, E. *Eur. J. Inorg. Chem.* **2013**, 2985-3007. (b) You, Y.; Park, S. Y. *Dalton Trans.* **2009**, 1267-1282.
[9] Rausch, A. F.; Thompson, M. E.; Yersin, H. *J. Phys. Chem. A* **2009**, *113*, 5927-5932.
[10] Baranoff, E.; Curchod, B. F. *Dalton Trans.* **2015**, *44*, 8318-8329.
[11] Sajoto, T.; Djurovich, P. I.; Tamayo, A.; Yousufuddin, M.; Bau, R.; Thompson, M. E.; Holmes, R. J.; Forrest, S. R. *Inorg. Chem.* **2005**, *44*, 7992-8003.
[12] Yang, C.-H.; Mauro, M.; Polo, F.; Watanabe, S.; Muenster, I.; Fröhlich, R.; De Cola, L. *Chem. Mater.* **2012**, *24*, 3684-3695.
[13] You, Y.; Kim, K. S.; Ahn, T. K.; Kim, D.; Park, S. Y. *J. Phys. Chem. C* **2007**, *111*, 4052-4060.
[14] Chao, K.; Shao, K.; Peng, T.; Zhu, D.; Wang, Y.; Liu, Y.; Su, Z.; Bryce, M. R. *J. Mater. Chem. C* **2013**, *1*, 6800-6806.
[15] (a) Marchi, E.; Sinisi, R.; Bergamini, G.; Tragni, M.; Monari, M.; Bandini, M.; Ceroni, P. *Chem. Eur. J.* **2012**, *18*, 8765-8773. (b) You, Y.; Seo, J.; Kim, S. H.; Kim, K. S.; Ahn, T. K.; Kim, D.; Park, S. Y. *Inorg. Chem.* **2008**, *47*, 1476-1487.
[16] Kim, J. B.; Han, S. H.; Yang, K.; Kwon, S. K.; Kim, J. J.; Kim, Y. H. *Chem. Commun.* **2015**, *51*, 58.
[17] Fan, C.; Li, Y.; Yang, C.; Wu, H.; Qin, J.; Cao, Y. *Chem. Mater.* **2012**, *24*, 4581.
[18] Benjamin, H.; Zheng, Y.; Batsanov, A. S.; Fox, M. A.; Al-Attar, H. A.; Monkman, A. P.; Bryce, M. R. *Inorg. Chem.* **2016**, *55*, 8612.
[19] Hoveyda, H. R.; Karunaratne, V.; Rettig, S. J.; Orvig, C. *Inorg. Chem.* **1992**, *31*, 5408-5416.
[20] Brain, C. T.; Paul, J. M. *Synlett* **1999**, 1642-1644.
[21] Nonoyama, M. *Bull. Chem. Soc. Jpn.* **1974**, *47*, 767-768.
[22] Baranoff, E.; Curchod, B. F.; Frey, J.; Scopelliti, R.; Kessler, F.; Tavernelli, I.; Rothlisberger, U.; Gratzel, M.; Nazeeruddin, M. K. *Inorg. Chem.* **2012**, *51*, 215-224.
[23] Lamansky, S.; Djurovich, P.; Murphy, D.; Abdel-Razzaq, F.; Kwong, R.; Tsyba, I.; Bortz, M.; Mui, B.; Bau, R.; Thompson, M. E. *Inorg. Chem.* **2001**, *40*, 1704-1711.
[24] Hay, P. J. *J. Phys. Chem. A* **2002**, *106*, 1634-1641.
[25] Tsuboyama, A.; Iwawaki, H.; Furugori, M.; Mukaide, T.; Kamatani, J.; Igawa, S.; Moriyama, T.; Miura, S.; Takiguchi, T.; Okada, S.; Hoshino, M.; Ueno, K. *J. Am. Chem. Soc.* **2003**, *125*, 12971-12979.
[26] Langer, V.; Koos, M.; Gyepesova, D.; Sladkovicova, M.; Luston, J.; Kronek, *J. Acta Crystallogr. C* **2005**, *61*, o602-o606.
[27] Takizawa, S.; Shimada, K.; Sato, Y.; Murata, S. *Inorg. Chem.* **2014**, 53, 2983−2995. (b) Sun, Q.; Mosquera-Vazquez, S.; Lawson Daku, L. M.; Guenee, L.; Goodwin, H. A.; Vauthey, E.; Hauser, A. *J. Am. Chem. Soc.* **2013**, 135, 13660−13663.
[28] Sheldrick, G. *Acta Crystallogr. A* **2008**, *64*, 112-122.
[29] Burla, M. C.; Caliandro, R.; Camalli, M.; Carrozzini, B.; Cascarano, G. L.; De Caro, L.; Giacovazzo, C.; Polidori, G.; Siliqi, D.; Spagna, R. *J. Appl. Crystallogr.* **2007**, *40*, 609-613.
[30] Dolomanov, O. V.; Bourhis, L. J.; Gildea, R. J.; Howard, J. A. K.; Puschmann, H. *J. Appl. Crystallogr.* **2009**, *42*, 339-341.
[31] Sheldrick, G. *Acta Crystallogr. C* **2015**, *71*, 3-8.

Insert Table of Contents artwork here

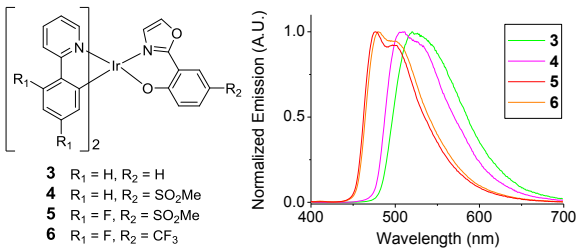

Supporting Information

Color Tuning of Efficient Electroluminescence in the Blue and Green Regions Using Heteroleptic Iridium Complexes with 2-Phenoxyoxazole Ancillary Ligands

Helen Benjamin,[†] Jie Liang,[§] Yu Liu,*[,§] Yun Geng,[‡] Xingman Liu,[‡] Dongxia Zhu,*[,‡] Andrei S. Batsanov,[†] and Martin R. Bryce*[,†]

[†]Department of Chemistry, Durham University, Durham DH1 3LE, U.K.

[§]State Key Laboratory of Supramolecular Structure and Materials, College of Chemistry, Jilin University, Changchun 130012, P.R. China

[‡]Key Laboratory of Nanobiosensing and Nanobioanalysis at Universities of Jilin Province, Department of Chemistry, Northeast Normal University, 5268 Renmin Street, Changchun, Jilin Province 130024, P.R. China

E-mails: m.r.bryce@durham.ac.uk; yuliu@jlu.edu.cn; zhudx047@nenu.edu.cn

Contents

Calculated orbital contour plots for complexes 2’ and 6’

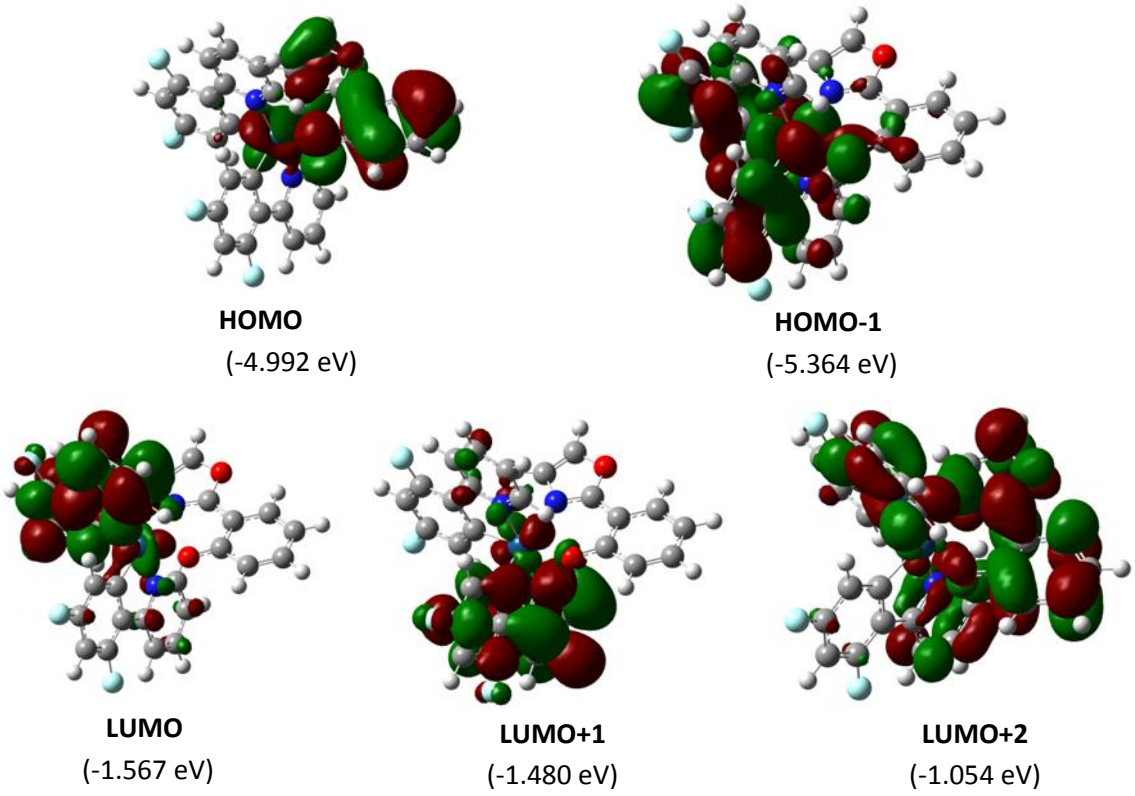

Figure S1. The contour plots of the HOMOs and LUMOs of complex **2’**.

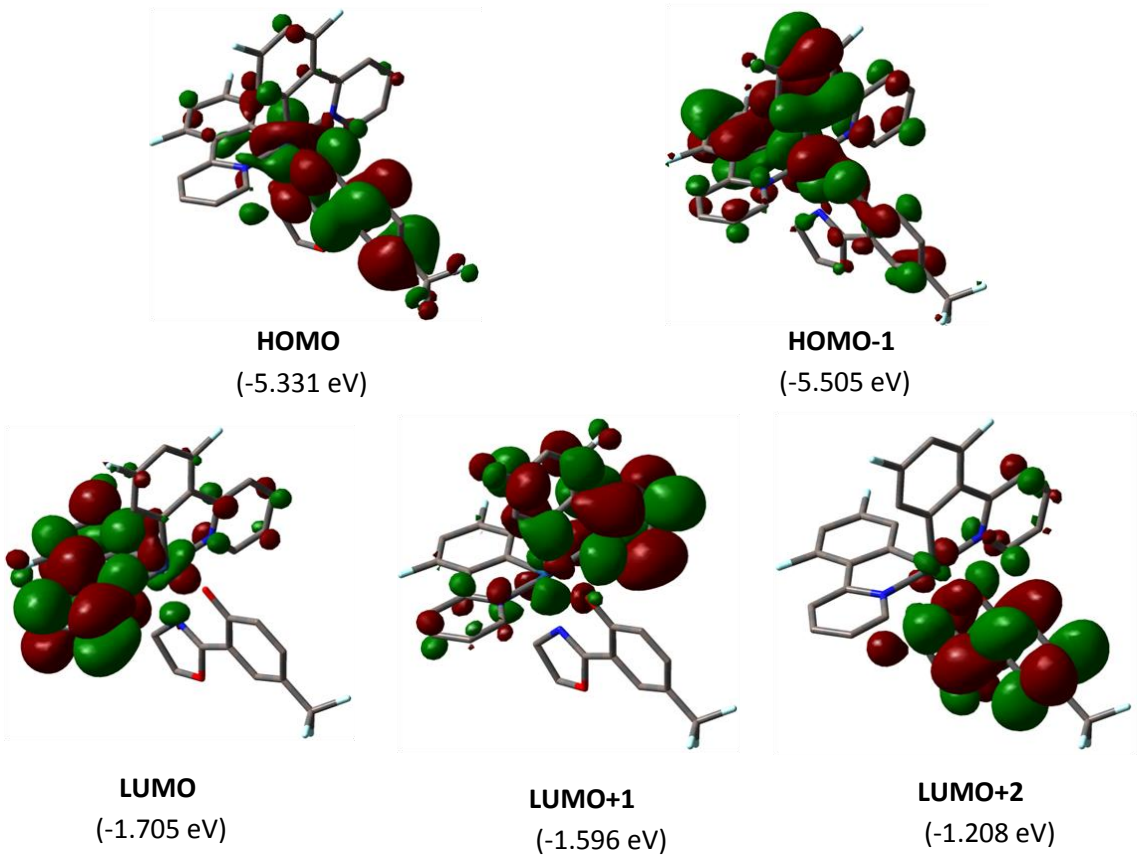

Figure S2. The contour plots of the HOMOs and LUMOs of complex **6'**.

X-ray crystallography

Table S1. Crystal data

Compound	**2**	**4**	**6**
CCDC	1512945	1512946	1512947
Formula	$C_{31}H_{20}F_4IrN_3O_2$ ·½ CH_2Cl_2	$C_{32}H_{24}IrN_3O_4S$ ·2C_4H_8O	$C_{32}H_{17}F_7IrN_3O_2$·0.4 CH_2Cl_2·0.1 $CHCl_3$
$D_{calc.}$/ g cm^{-3}	1.879	1.655	1.947
μ/mm^{-1}	5.02	3.88	4.81
Formula Weight	777.16	883.01	846.59
Size/mm^3	0.23×0.21×0.18	0.22×0.21×0.20	0.29×0.21×0.19
T/K	293	120	120
Crystal System	monoclinic	monoclinic	triclinic
Space Group	C2/c	$P2_1/n$	P-1
a/Å	24.3108(14)	12.8946(5)	13.0961(6)
b/Å	15.9429(14)	16.5103(7)	14.9991(7)
c/Å	14.7716(10)	16.7577(7)	17.6182(9)
α/°	90	90	100.939(2)
β/°	106.302(2)	96.473(1)	105.983(2)
γ/°	90	90	112.871(2)
V/Å^3	5495.1(7)	3544.9(3)	2888.2(2)
Z	8	4	4
Wavelength/Å	0.71073	0.71073	0.71073
Θ_{max}/°	25.082	35.607	35.800
Measured Refls.	15352	96252	79318
Independent Refls.	4876	15430	24074
Refls. with I>2σ(I)	3983	13645	19800
R_{int}	0.035	0.027	0.028
Parameters/restraints	384, 0	467, 12	892, 46
wR_2 (all data)	0.066	0.037	0.054
R_1 [I>2σ(I)]	0.026	0.018	0.026

Thermal properties

Table S2. Thermal stability data for complexes **2-6**.

Complex	T_d (°C)[a]
2	308
3	320
4	310
5	311
6	304

[a] Defined as the 5% weight loss temperature.

Copies of NMR spectra

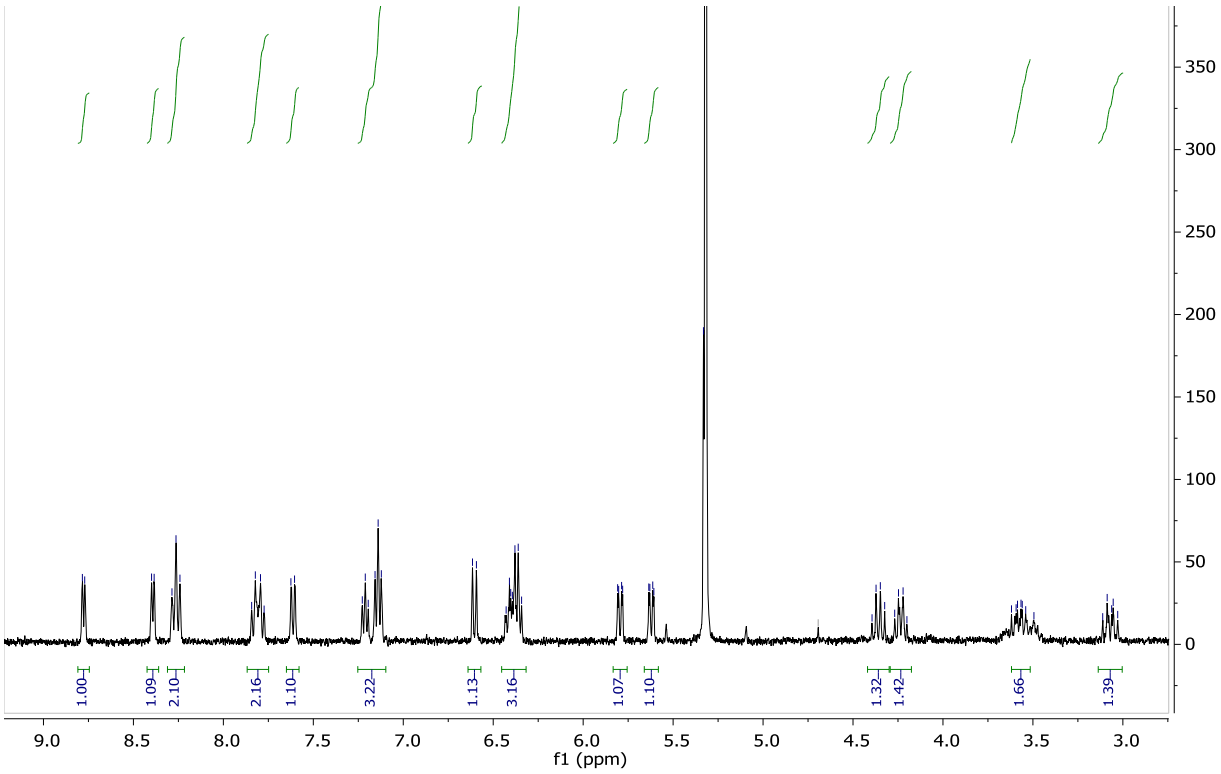

Figure S3. ^{1}H NMR spectrum of **2** in CD_2Cl_2.

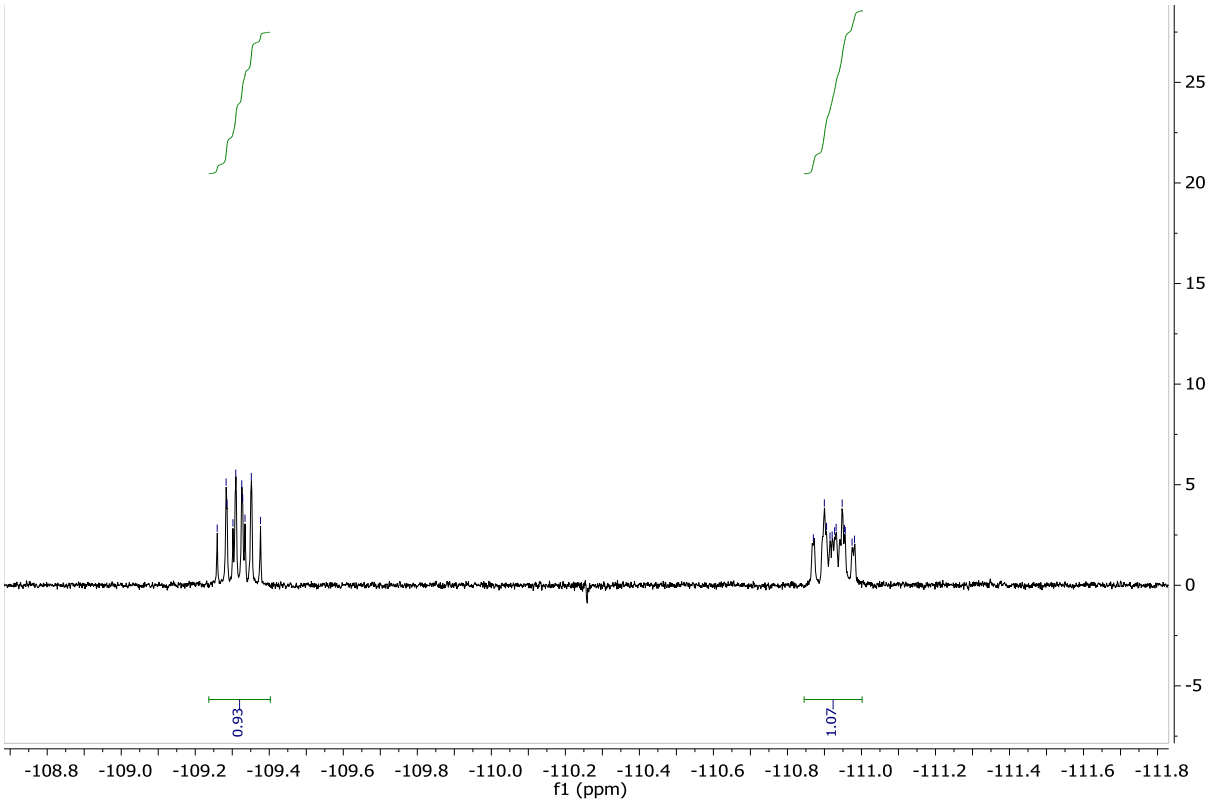

Figure S4. ^{19}F NMR spectrum of **2** in CD_2Cl_2.

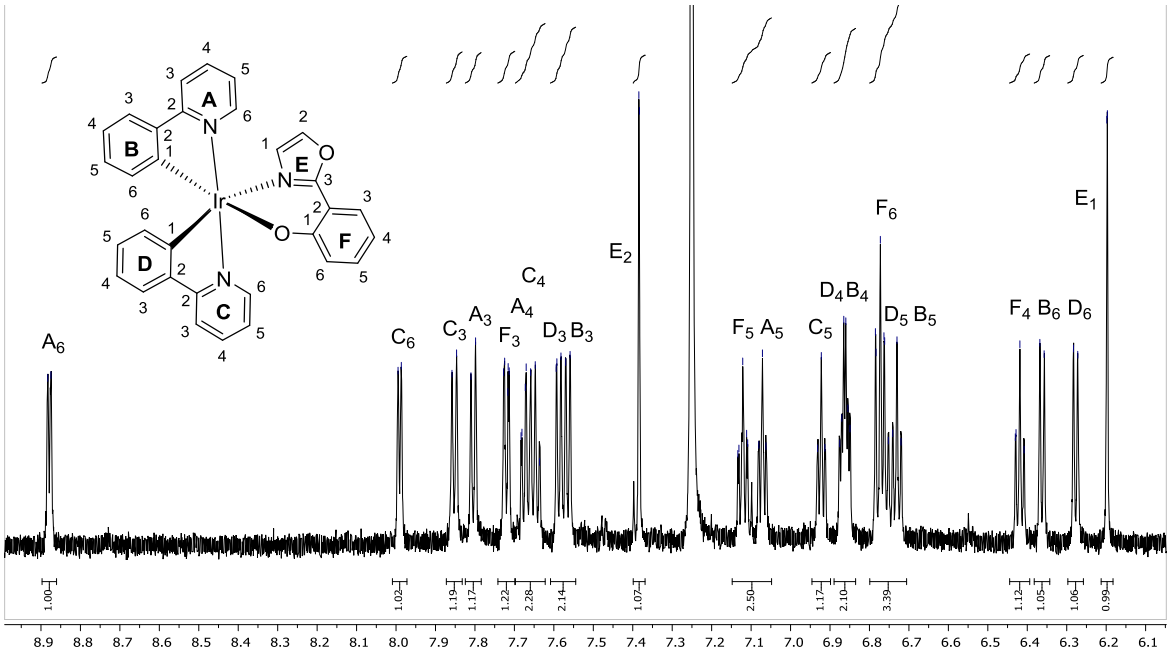

Figure S5. ^{1}H NMR spectrum of **3** in $CDCl_3$.

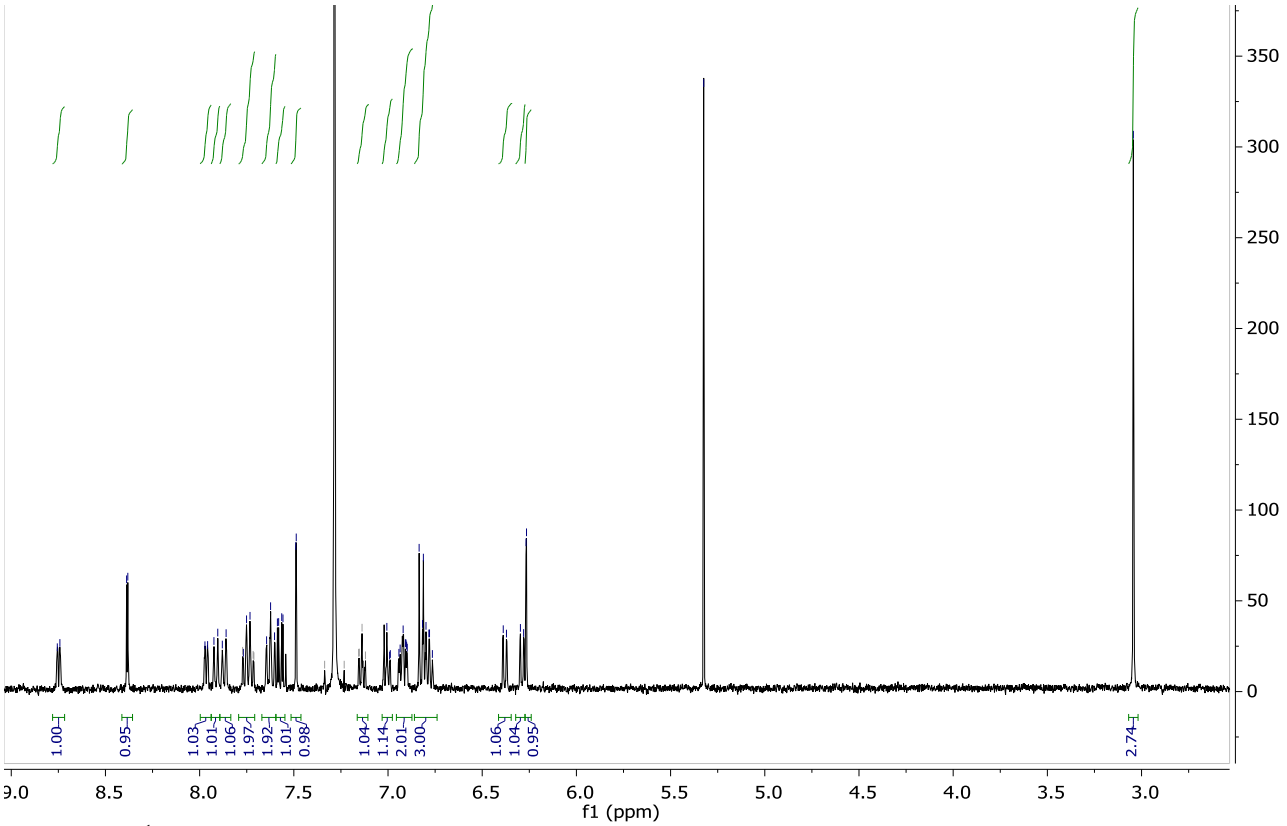

Figure S6. ^{1}H NMR spectrum of **4** in $CDCl_3$.

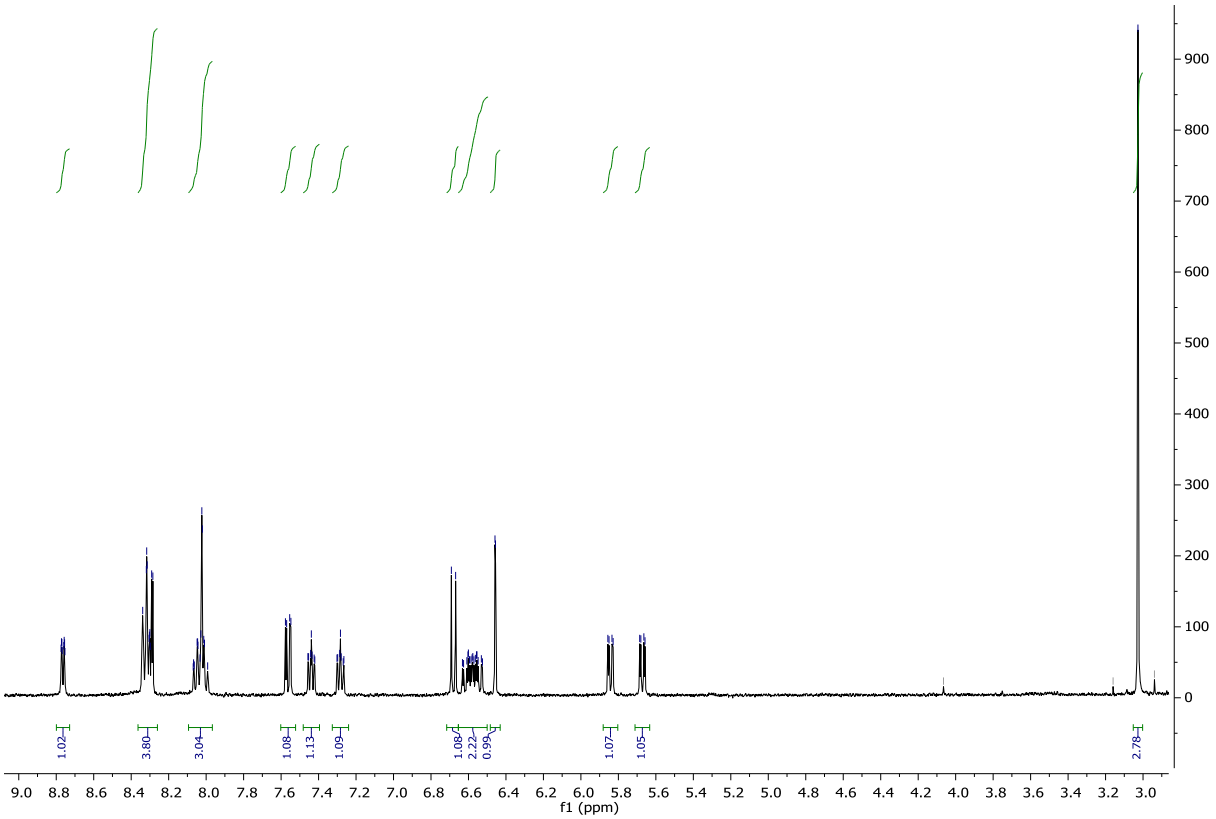

Figure S7. ^{1}H NMR spectrum of **5** in Acetone-d_6.

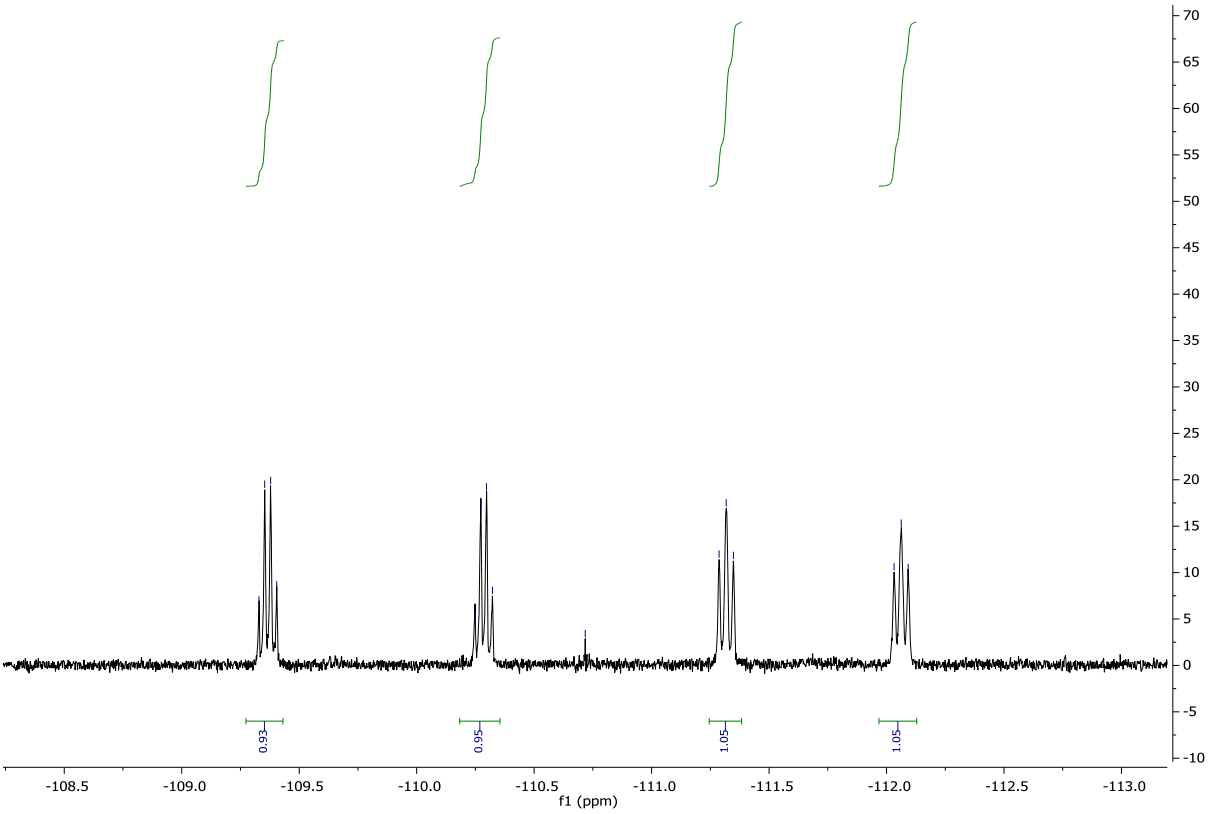

Figure S8. ^{19}F NMR spectrum of **5** in Acetone-d_6.

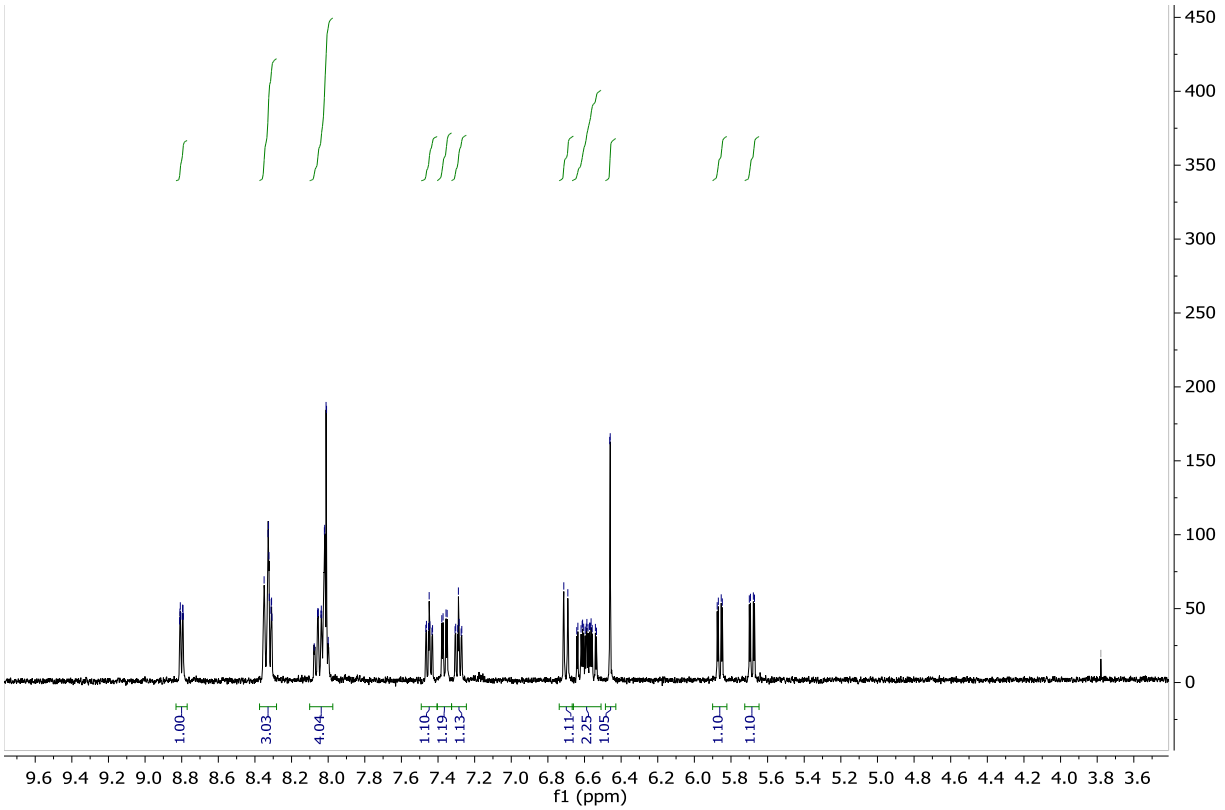

Figure S9. ^{1}H NMR spectrum of **6** in Acetone-d_6.

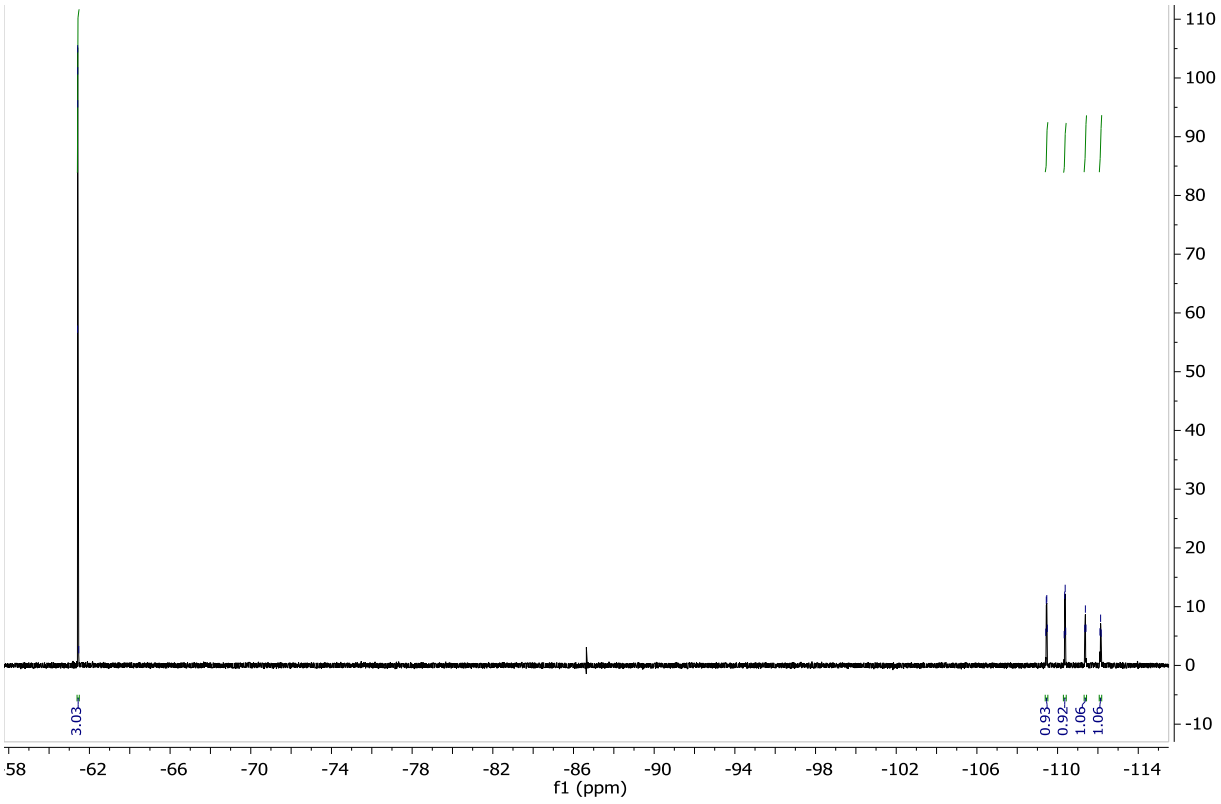

Figure S10. ^{19}F NMR spectrum of **6** in Acetone-d_6.

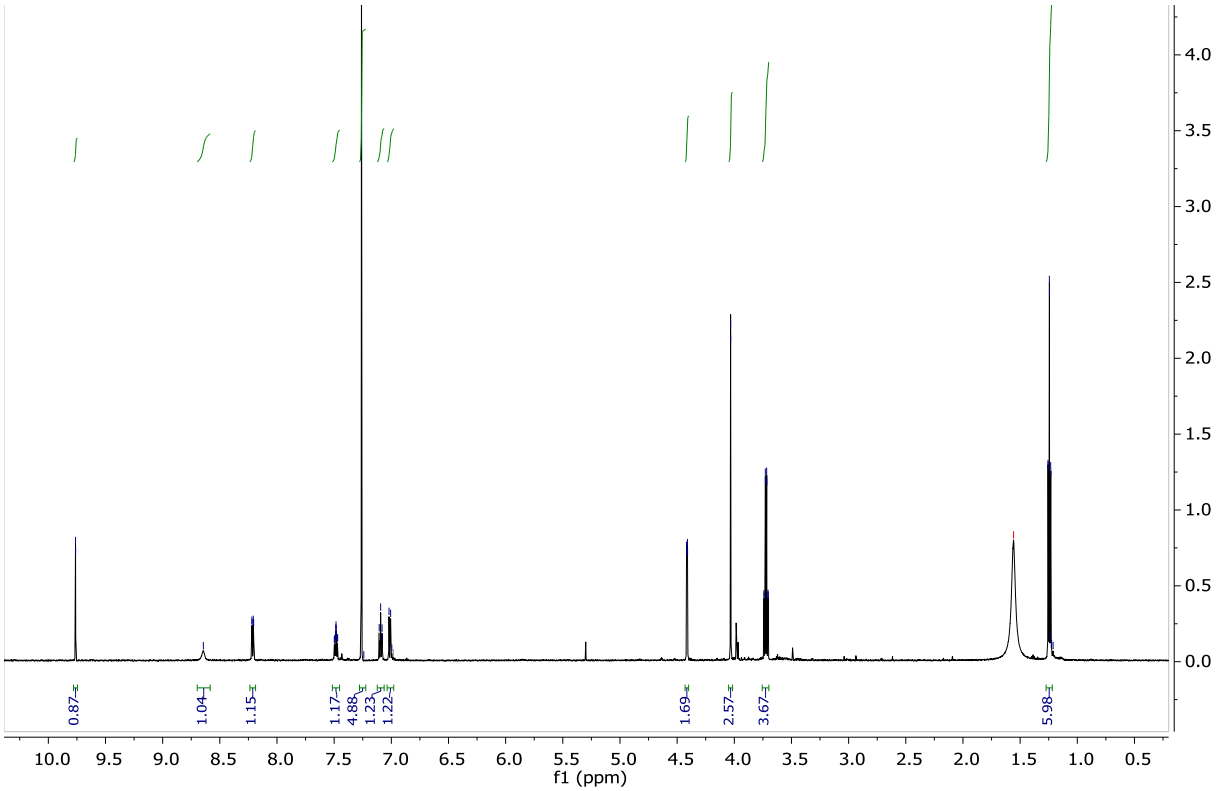

Figure S11. ^{1}H NMR spectrum of **8** in $CDCl_3$.

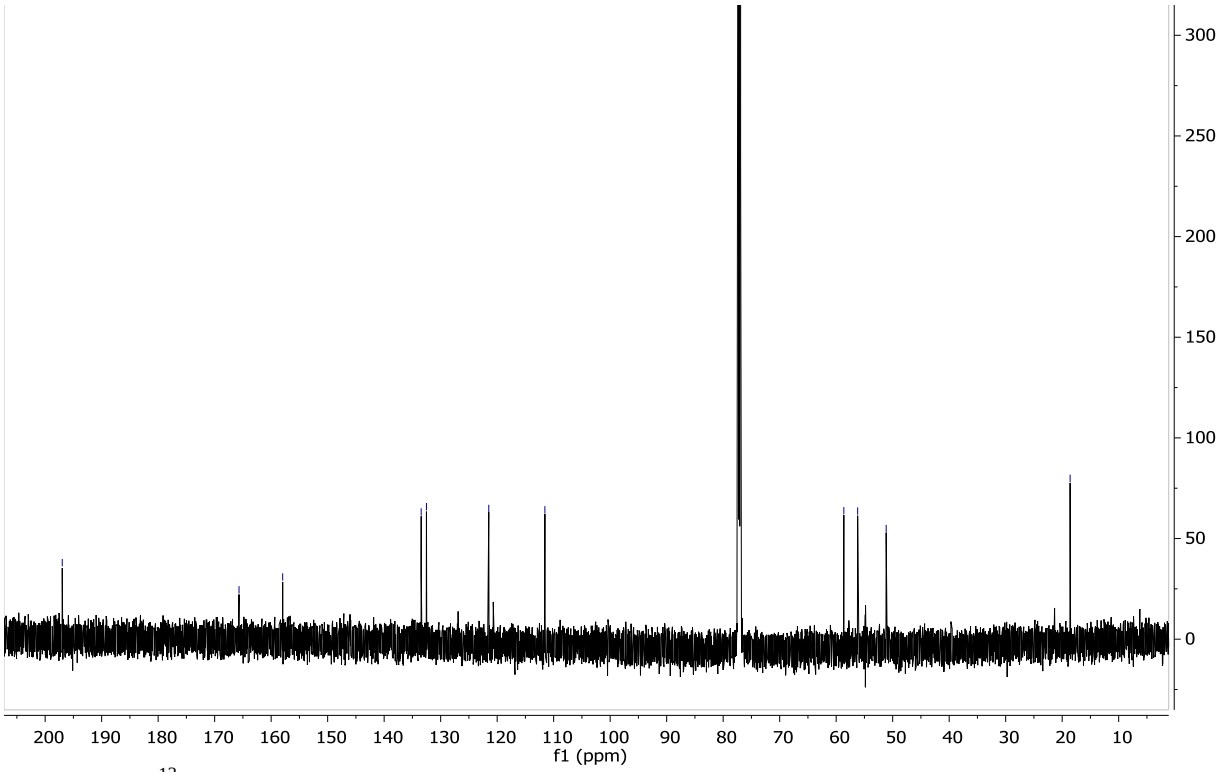

Figure S12. ^{13}C NMR spectrum of **8** in $CDCl_3$.

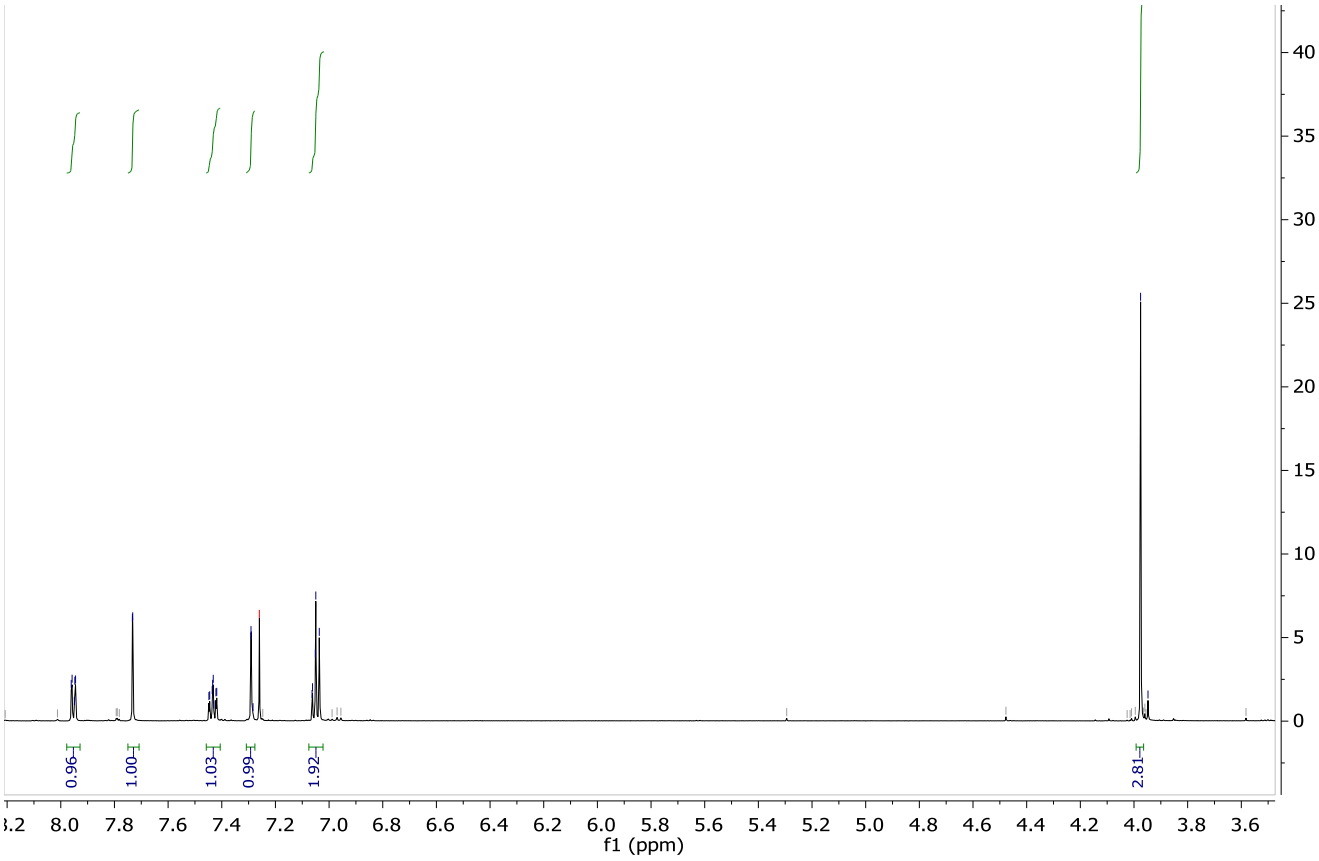

Figure S13. ^{1}H NMR spectrum of **9** in $CDCl_3$.

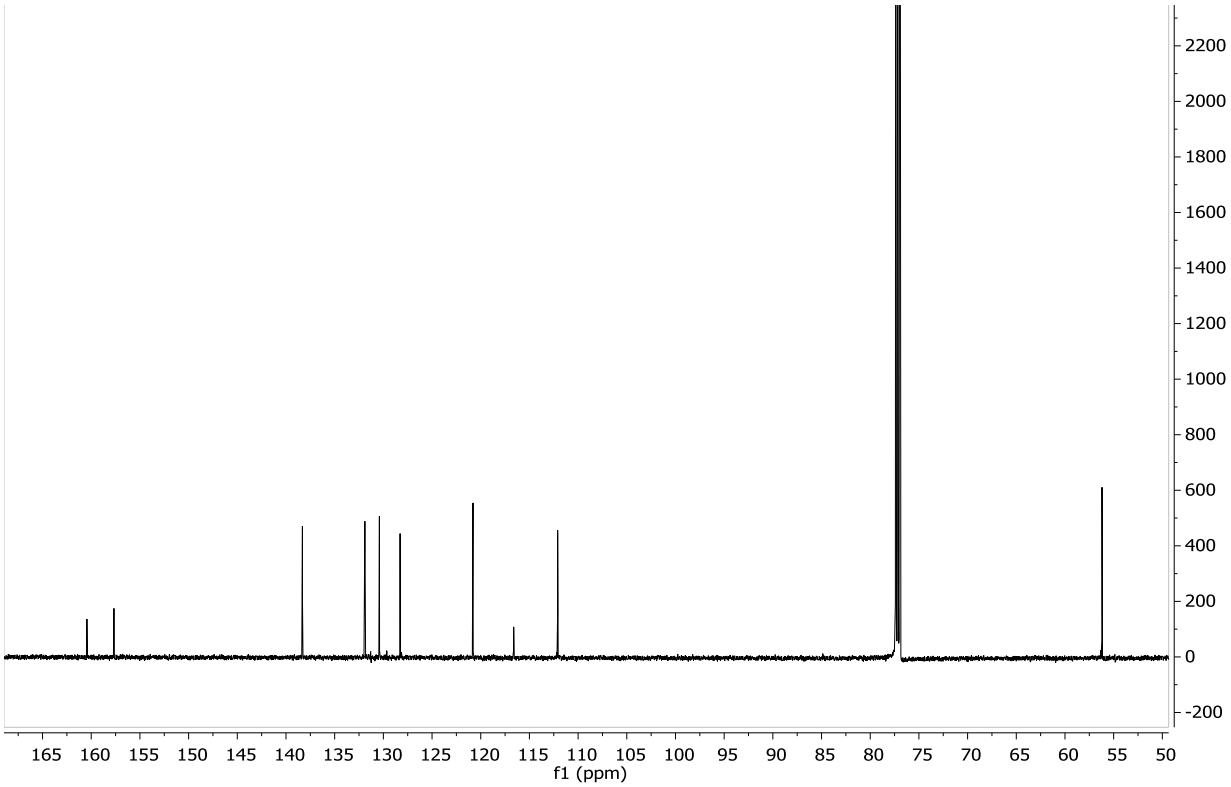

Figure S14. ^{13}C NMR spectrum of **9** in $CDCl_3$.

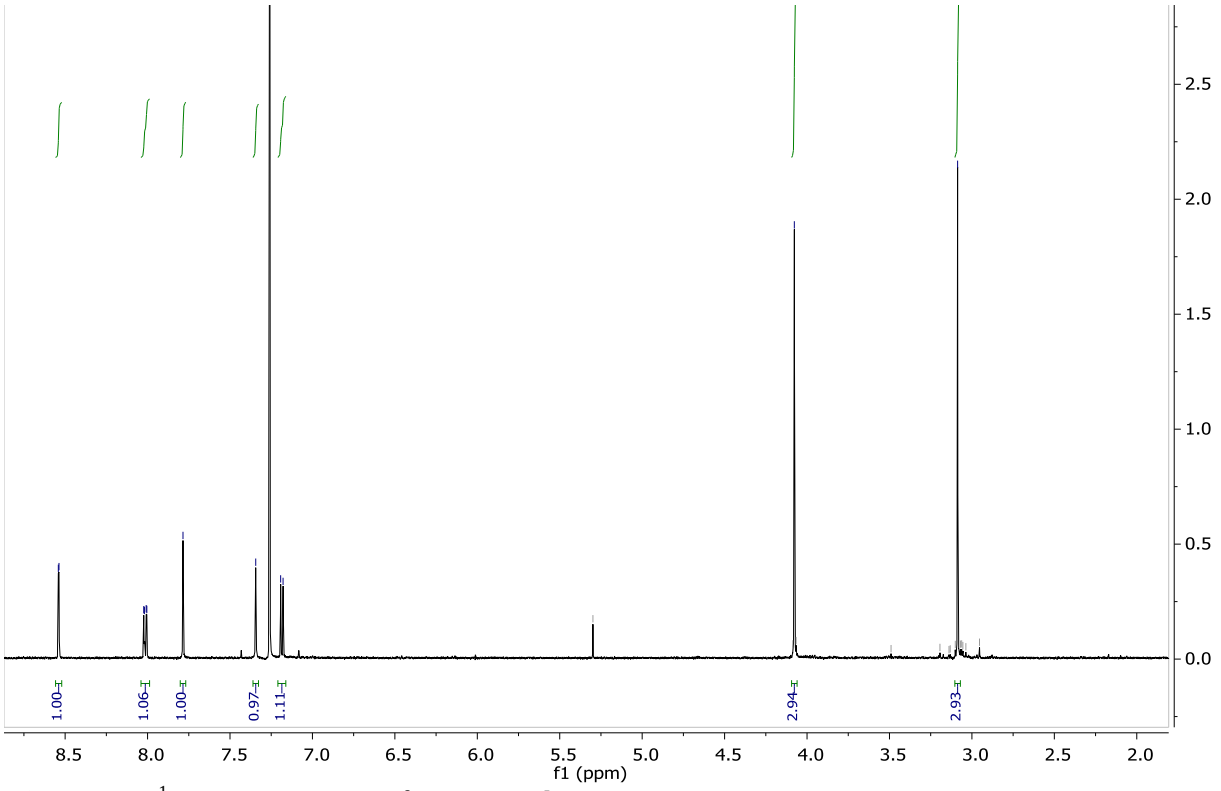

Figure S15. ^{1}H NMR spectrum of **10** in $CDCl_3$.

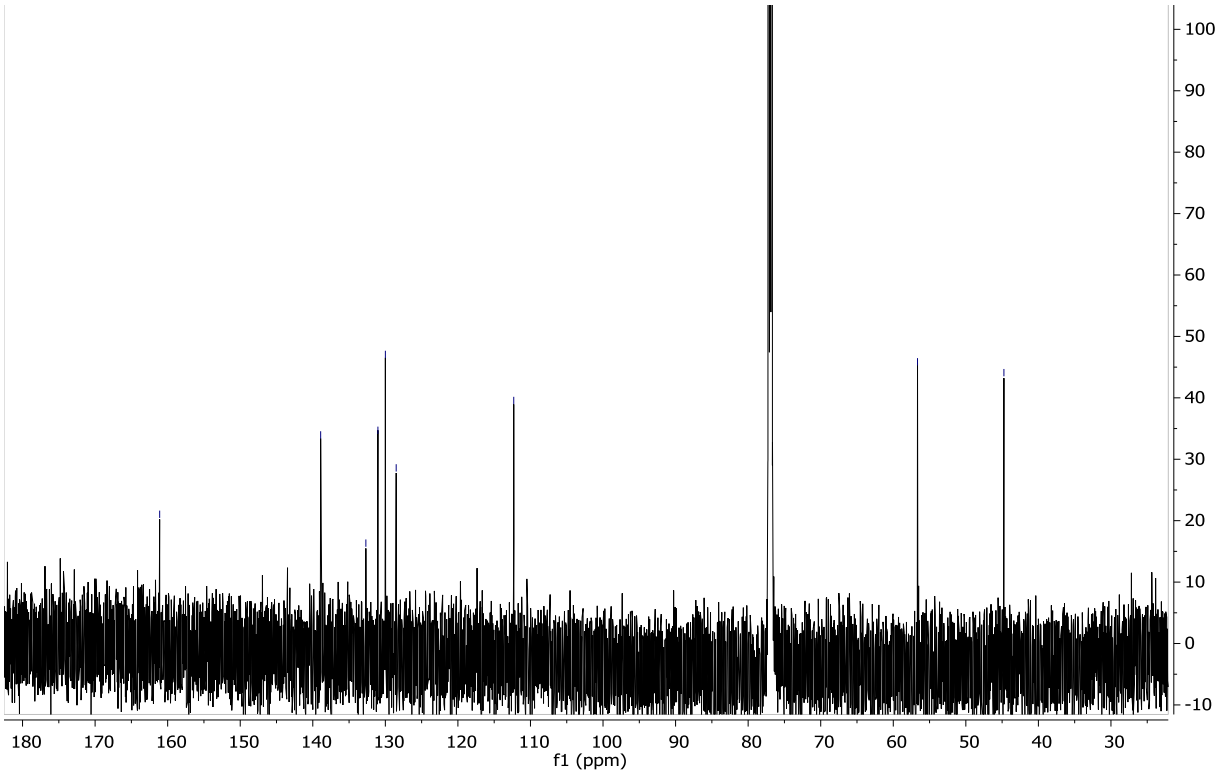

Figure S16. ^{13}C NMR spectrum of **10** in $CDCl_3$. Due to the low intensity of the ^{13}C spectrum the 2D NMR experiments have been included.

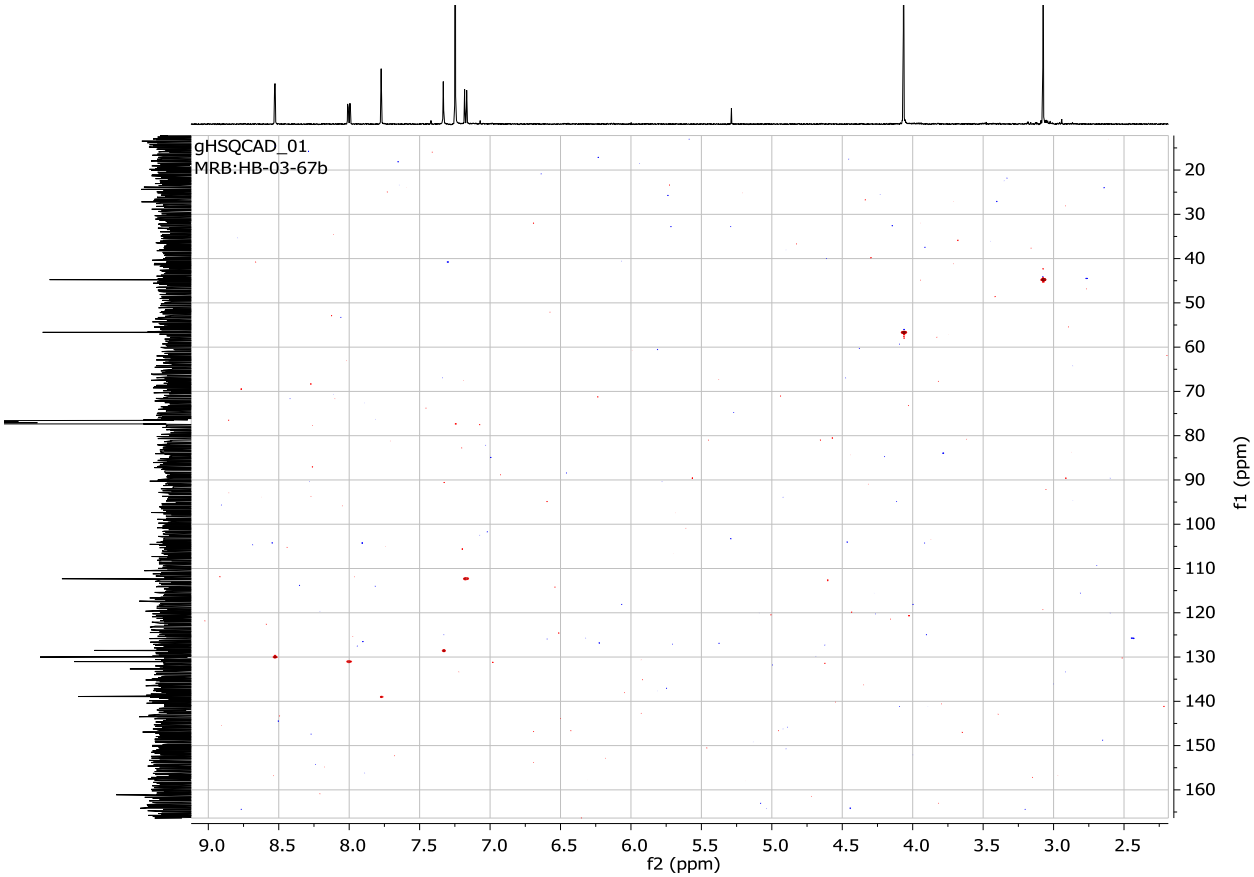

Figure S17. HSQC NMR spectrum of **10** in $CDCl_3$.

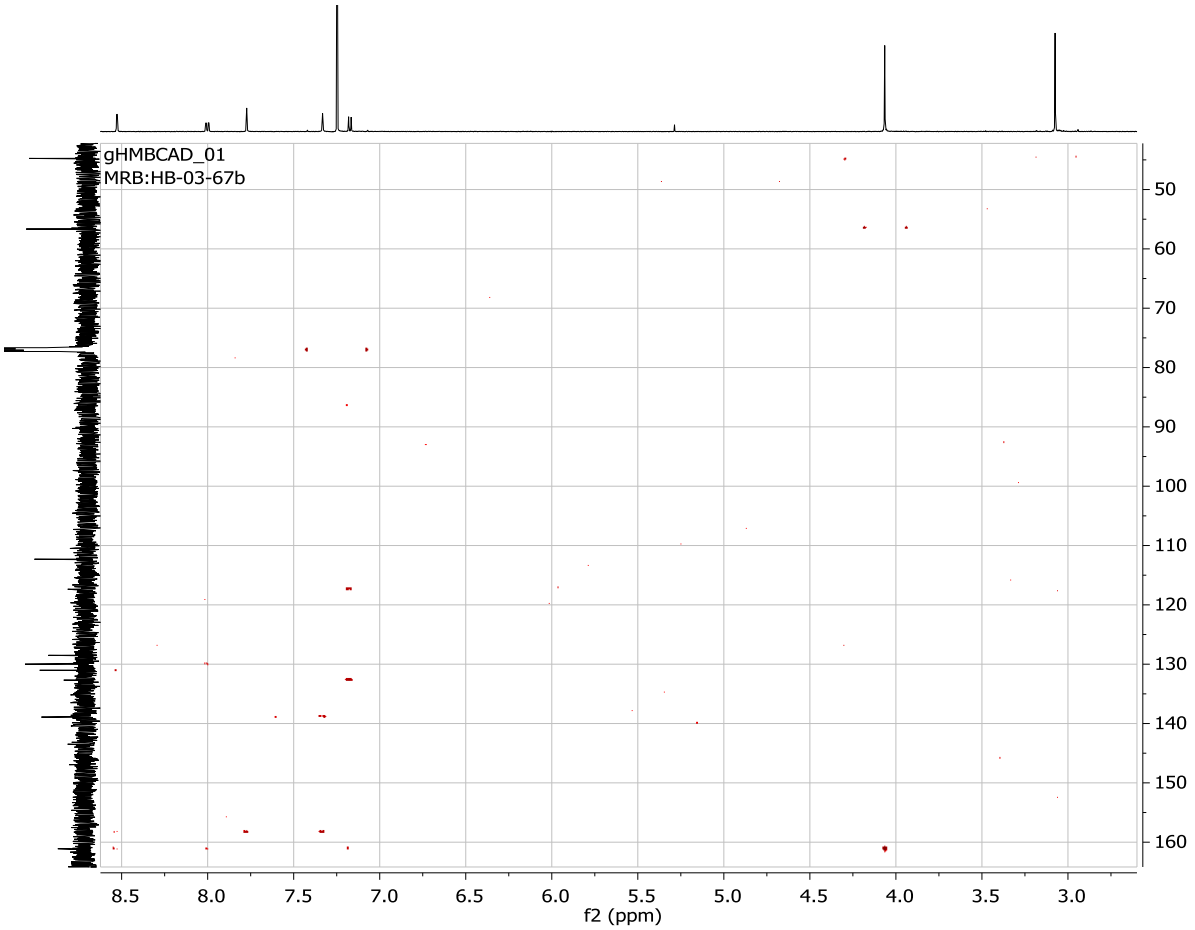

Figure S18. HMBC NMR spectrum of **10** in $CDCl_3$.

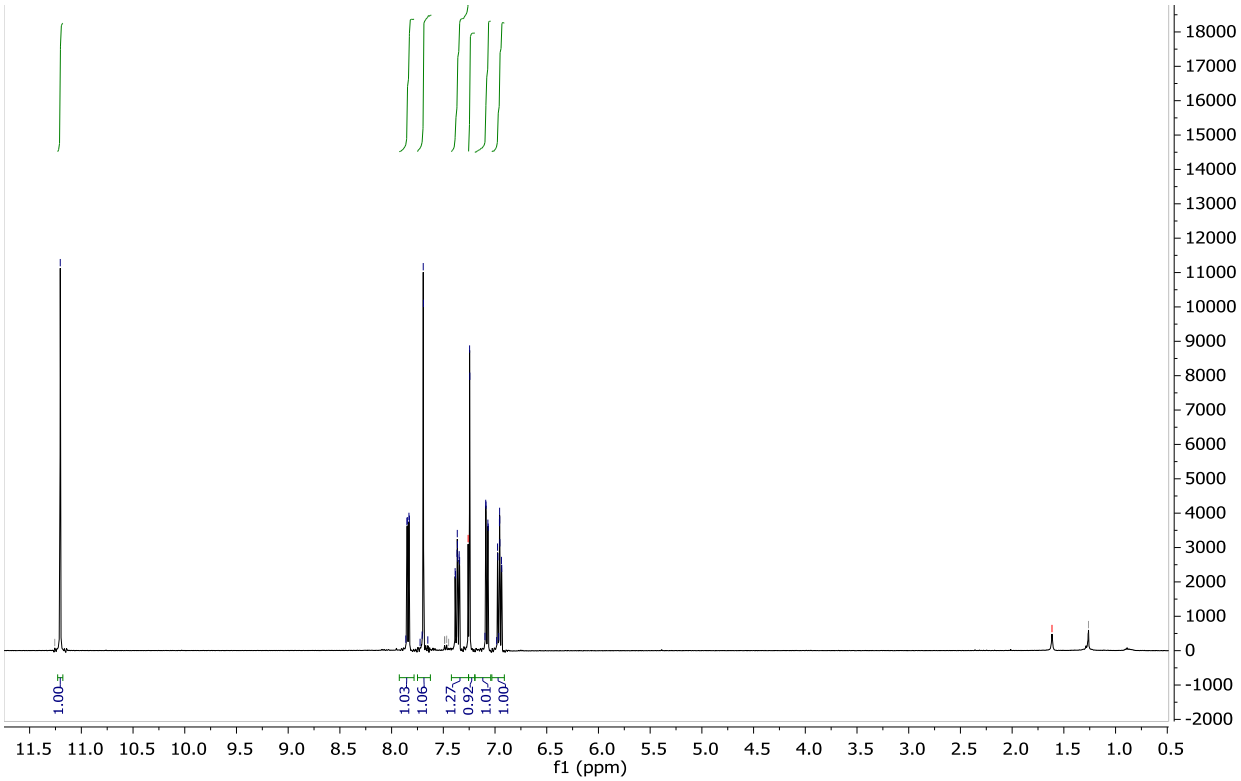

Figure S19. ^{1}H NMR spectrum of **11** in $CDCl_3$.

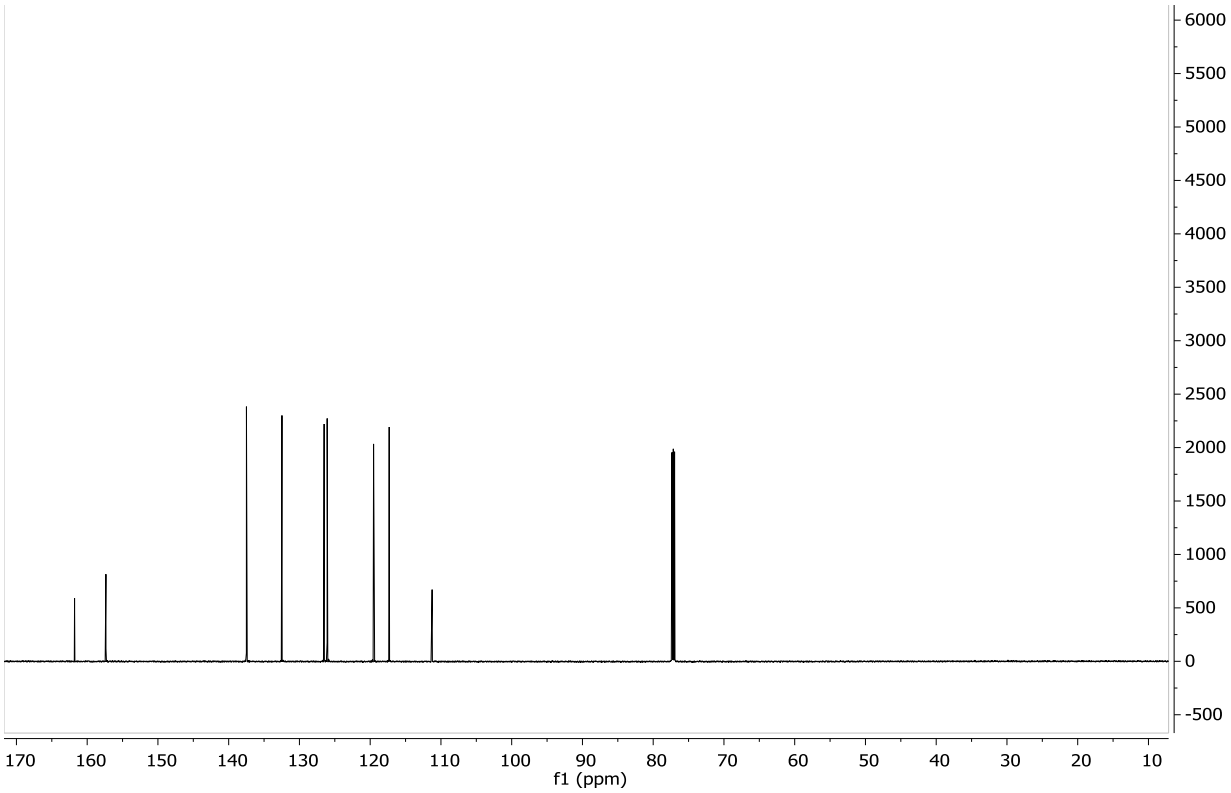

Figure S20. ^{13}C NMR spectrum of **11** in $CDCl_3$.

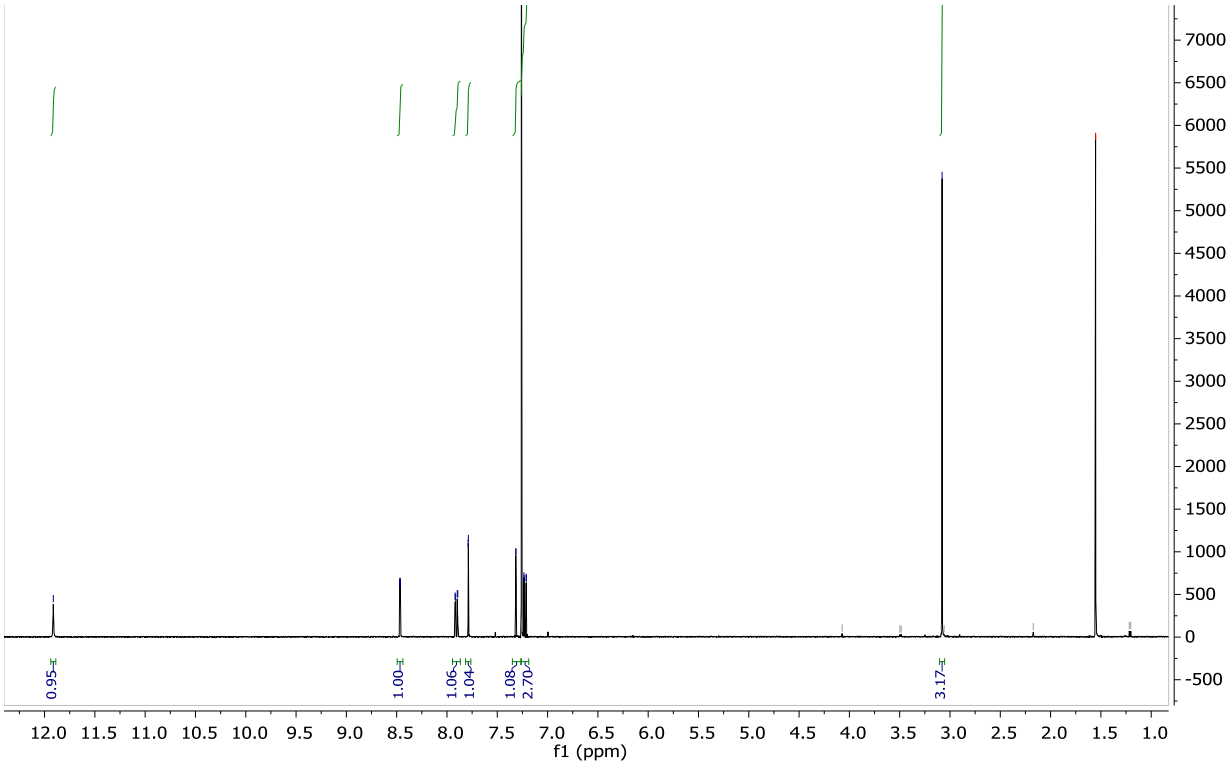

Figure S21. ^{1}H NMR spectrum of **12** in $CDCl_3$.

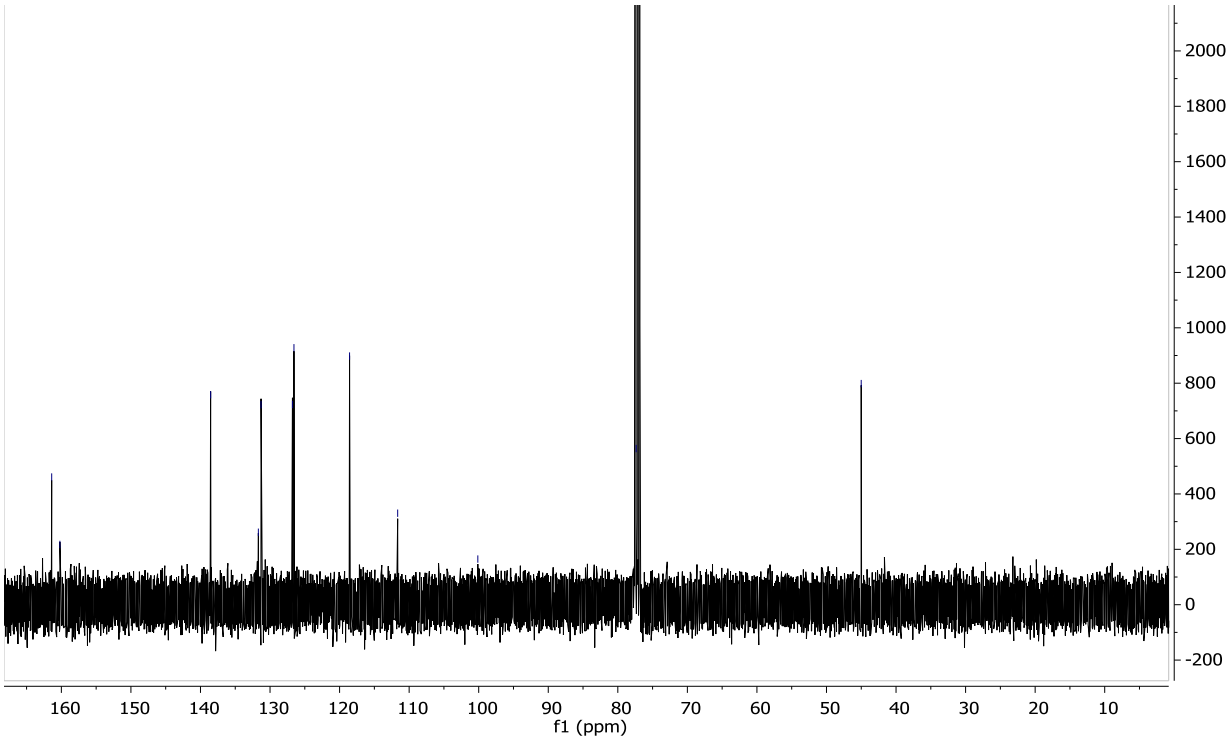

Figure S22. ^{13}C NMR spectrum of **12** in $CDCl_3$.

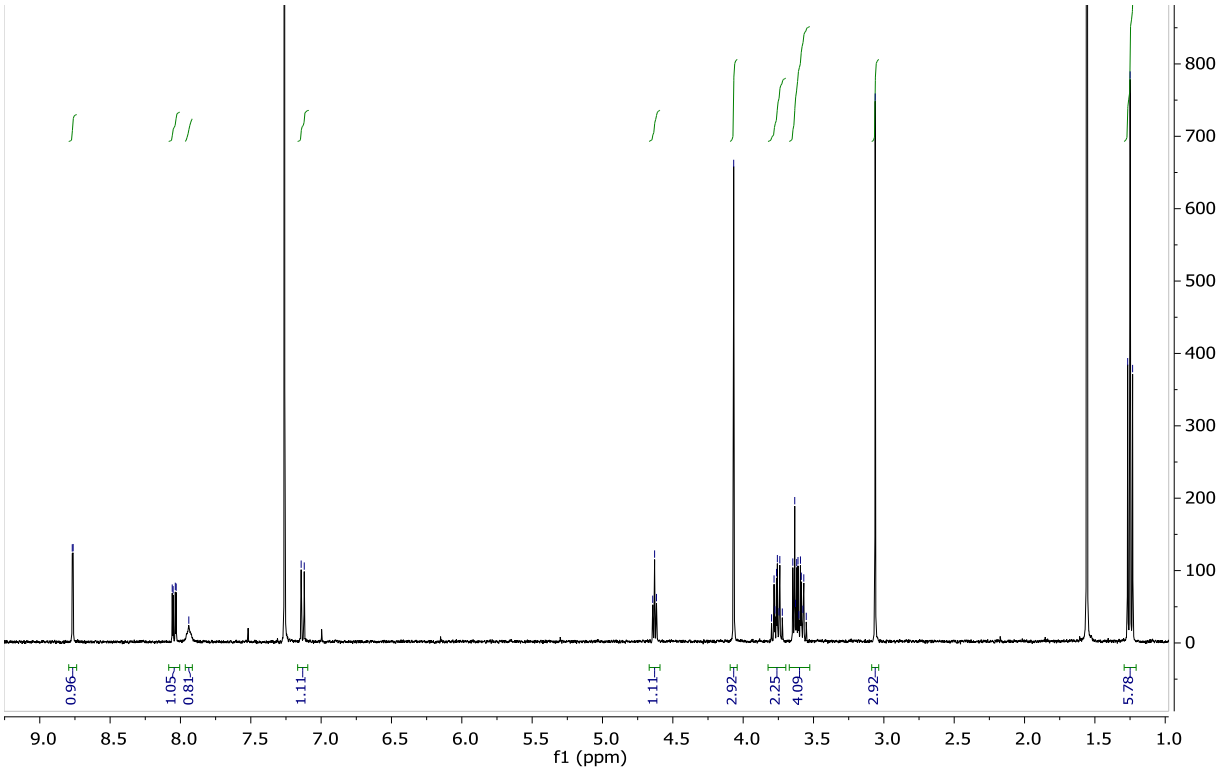

Figure S23. ^{1}H NMR spectrum of **15** in $CDCl_3$.

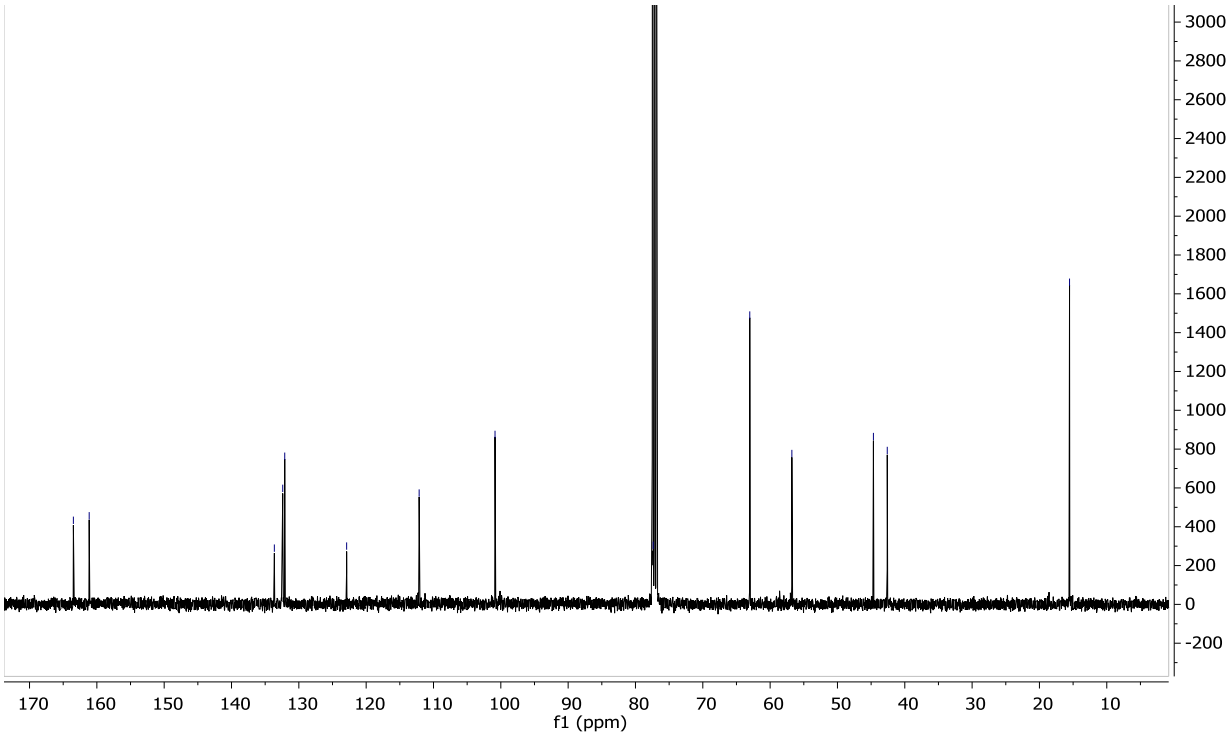

Figure S24. ^{13}C NMR spectrum of **15** in $CDCl_3$.

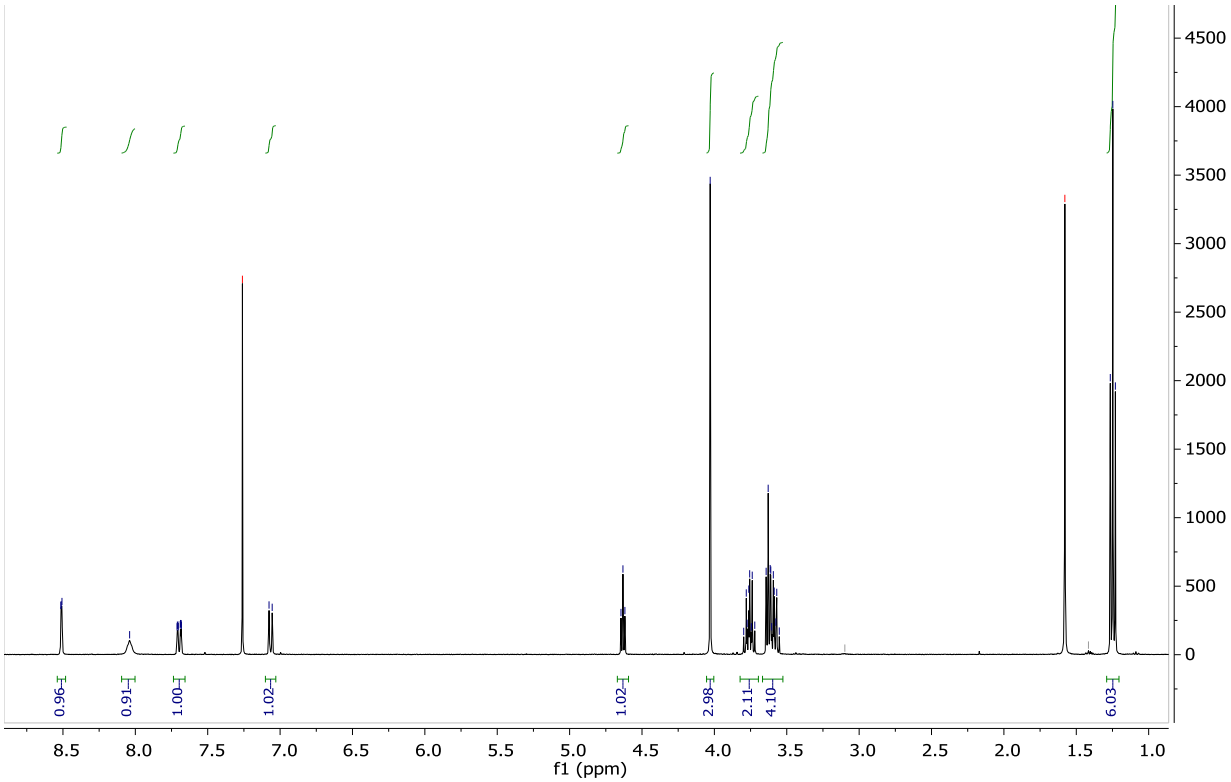

Figure S25. ^{1}H NMR spectrum of **16** in $CDCl_3$.

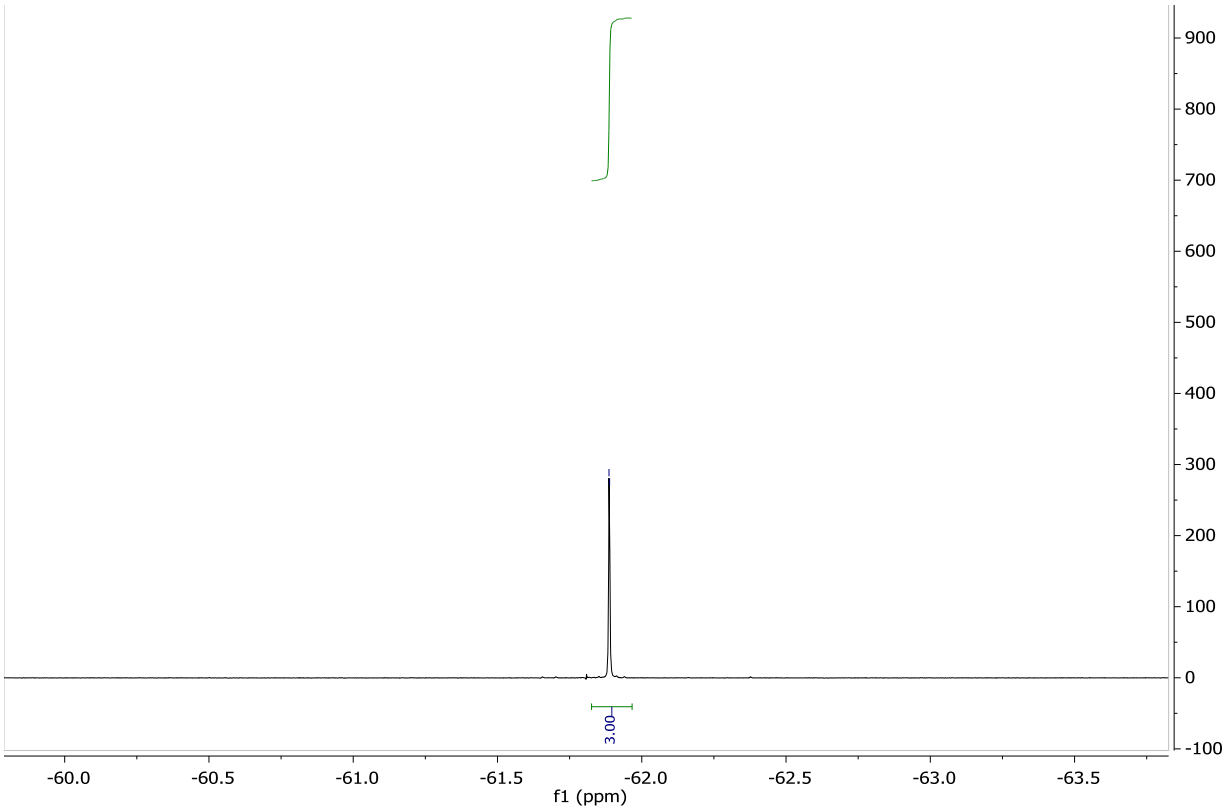

Figure S26. ^{19}F NMR spectrum of **16** in $CDCl_3$.

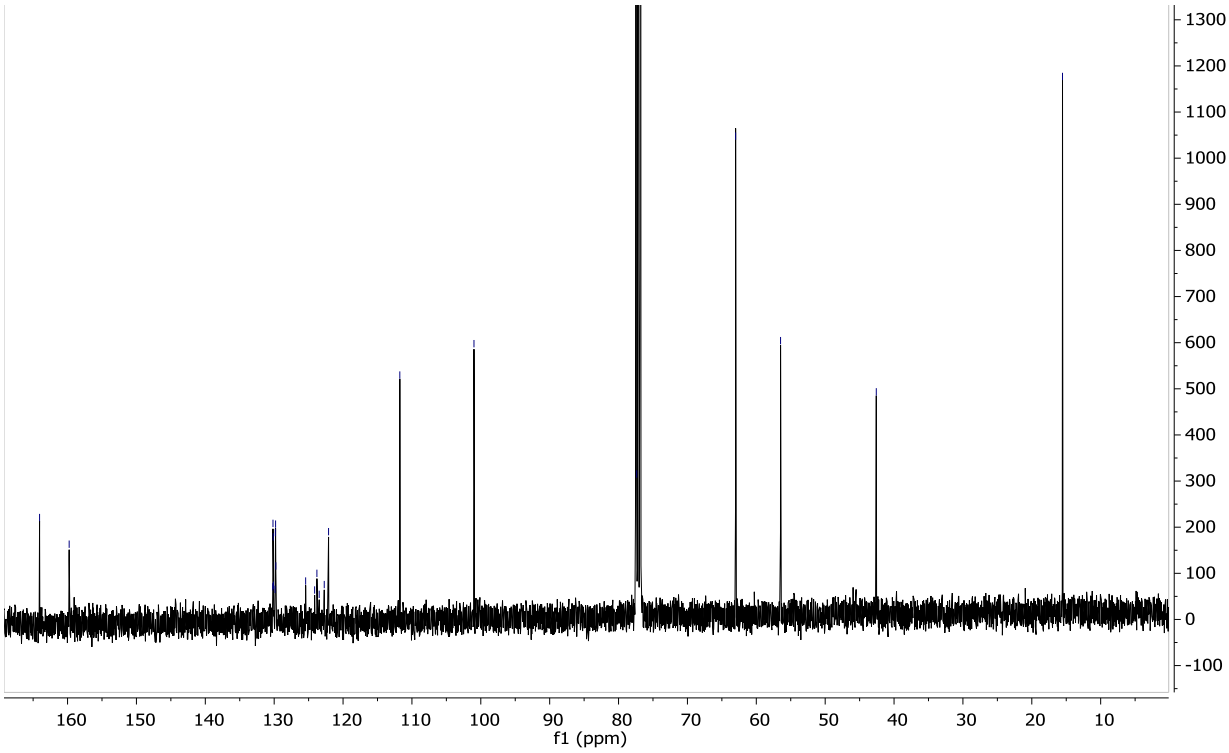

Figure S27. ^{13}C NMR spectrum of **16** in $CDCl_3$.

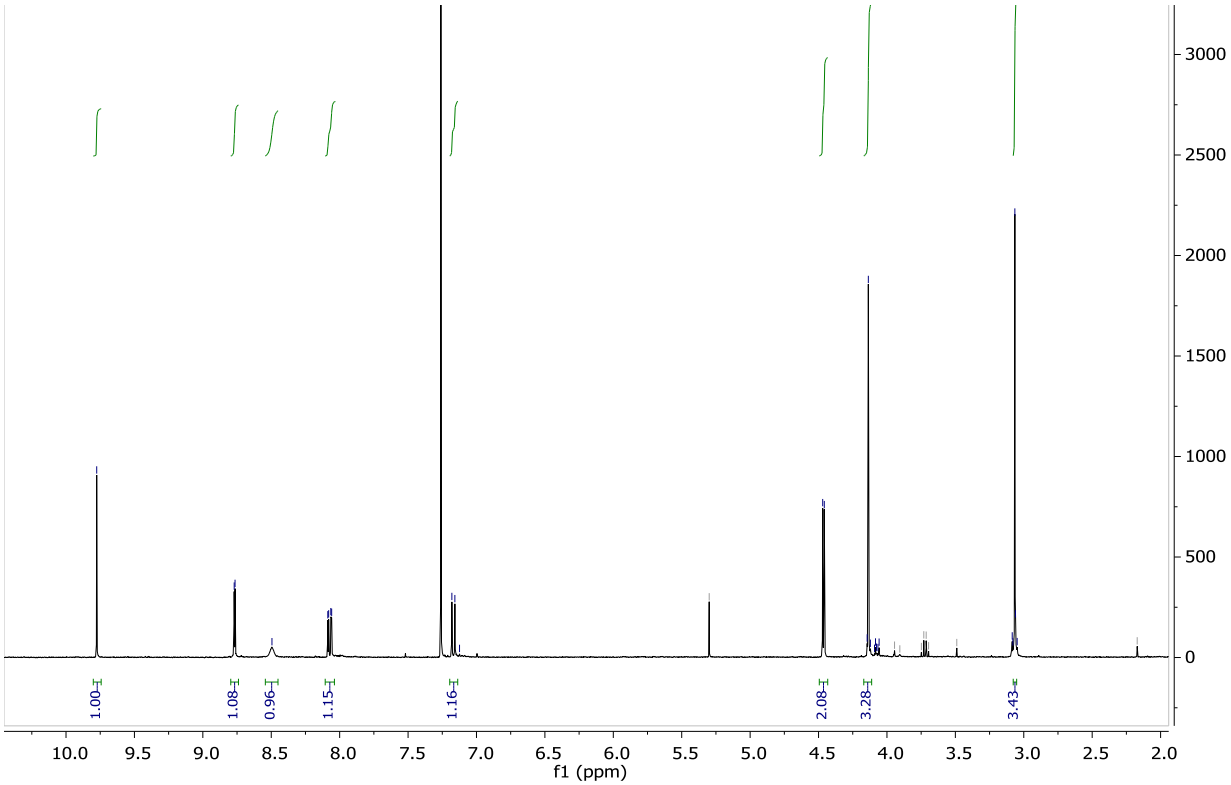

Figure S28. ^{1}H NMR spectrum of **17** in $CDCl_3$.

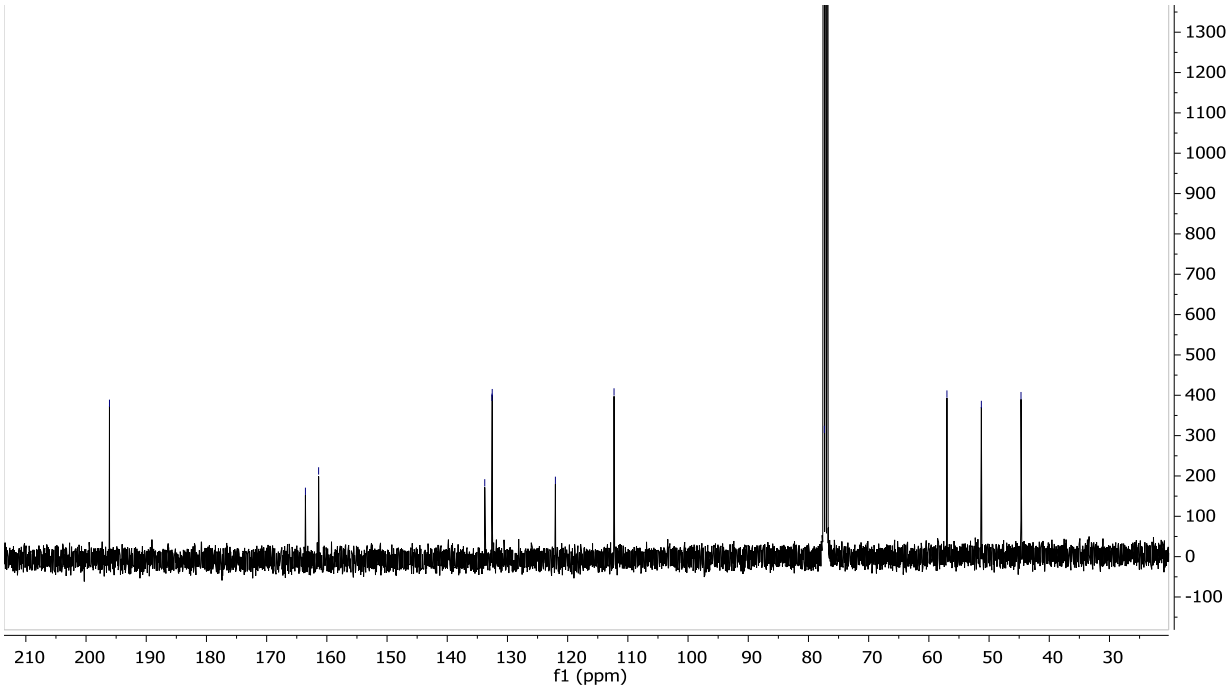

Figure S29. ^{13}C NMR spectrum of **17** in $CDCl_3$.

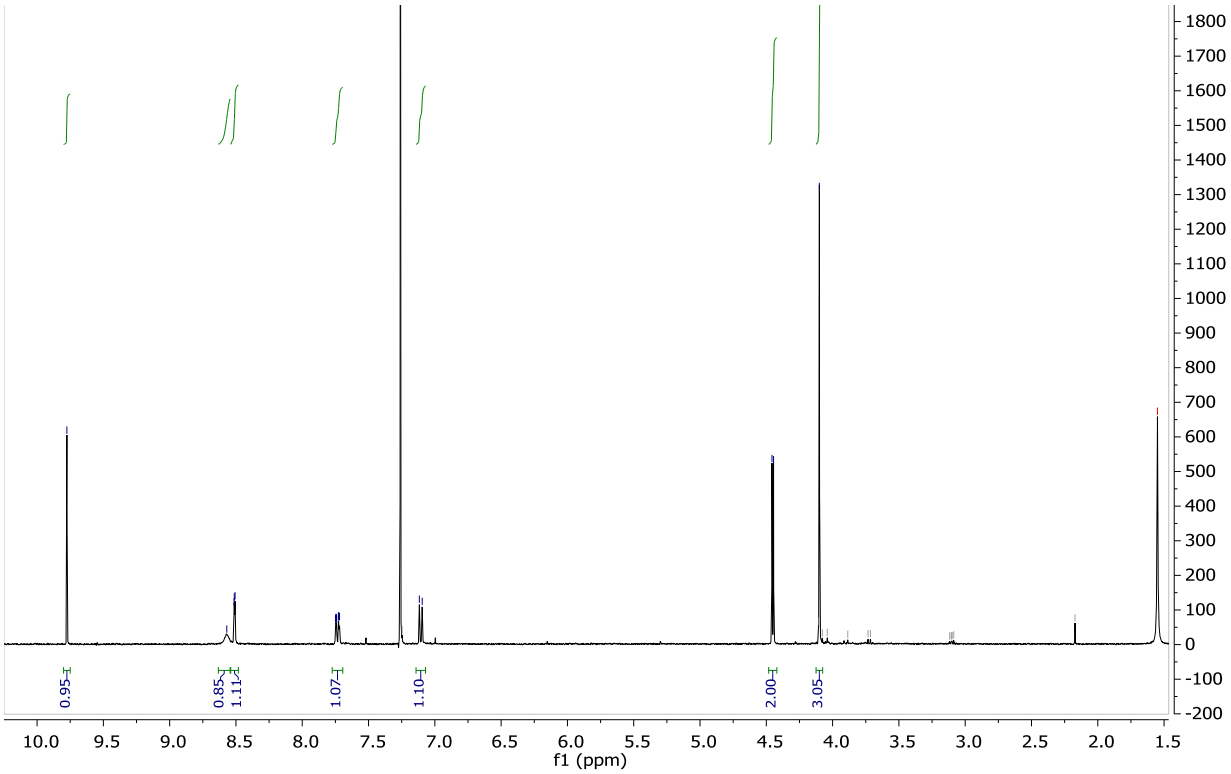

Figure S30. ^{1}H NMR spectrum of **18** in $CDCl_3$.

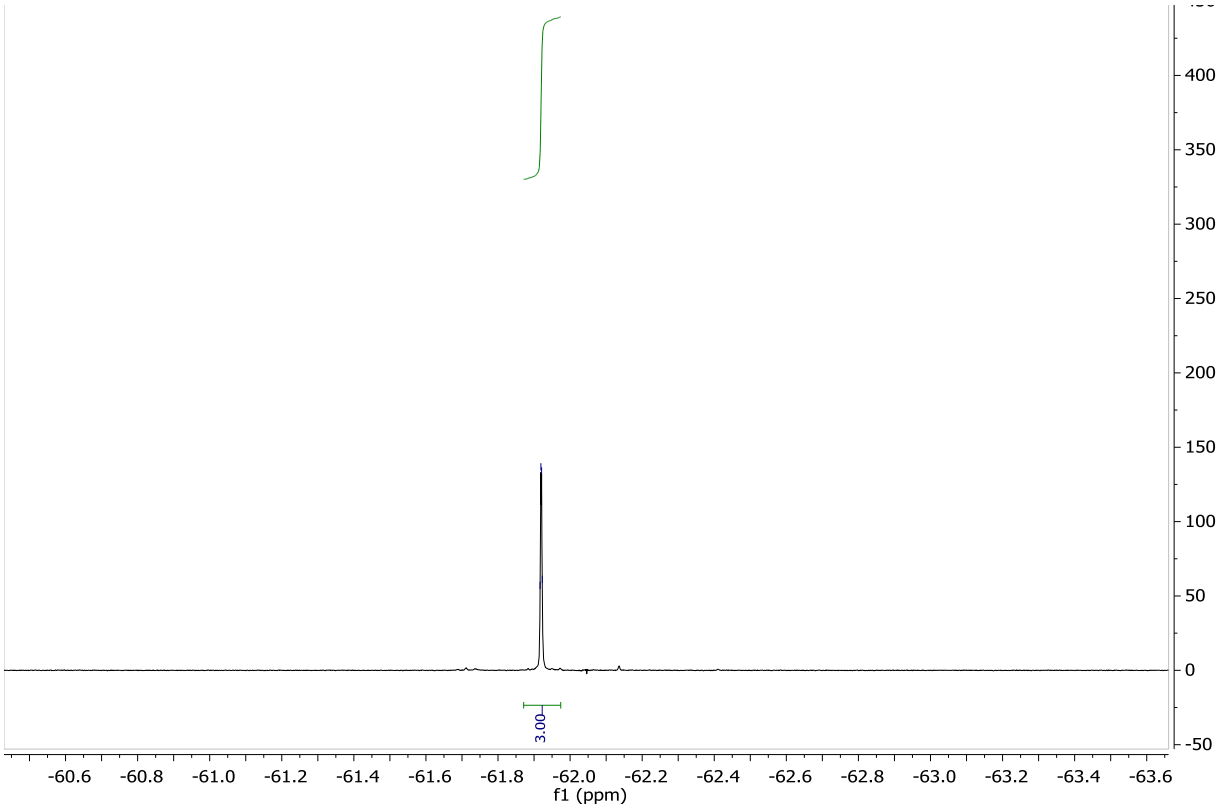

Figure S31. ^{19}F NMR spectrum of **18** in $CDCl_3$.

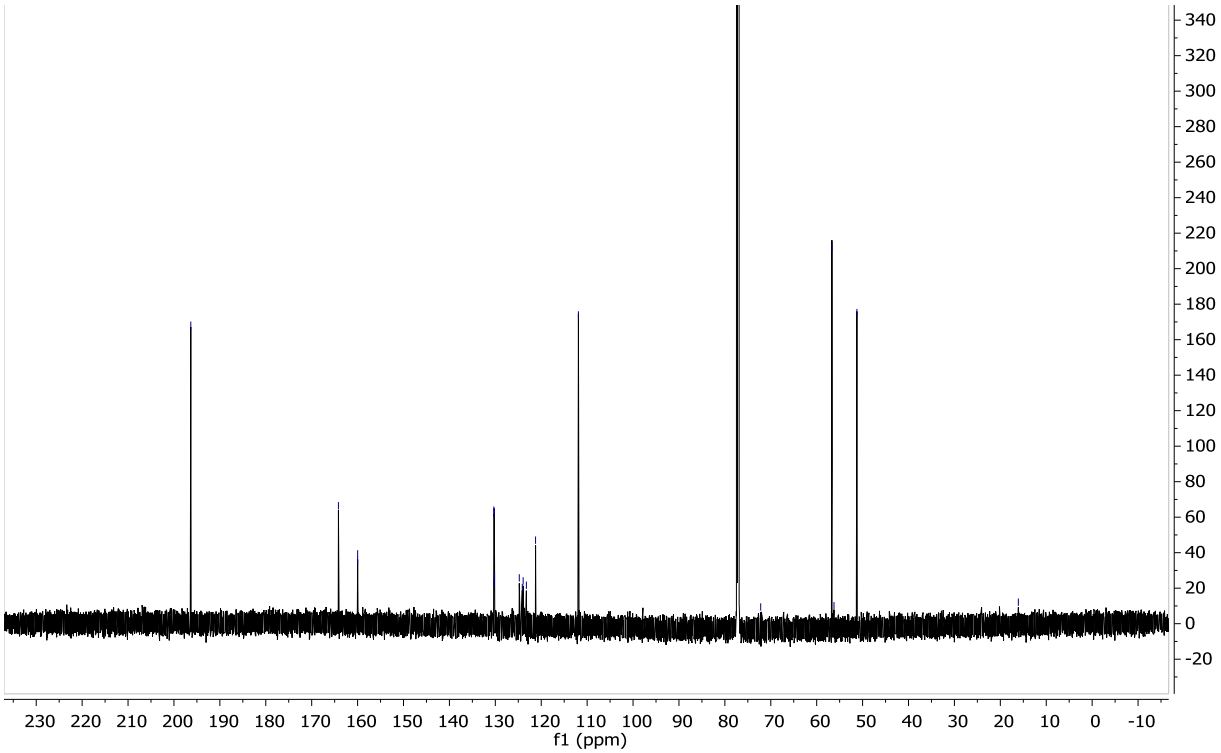

Figure S32. ^{13}C NMR spectrum of **18** in $CDCl_3$.

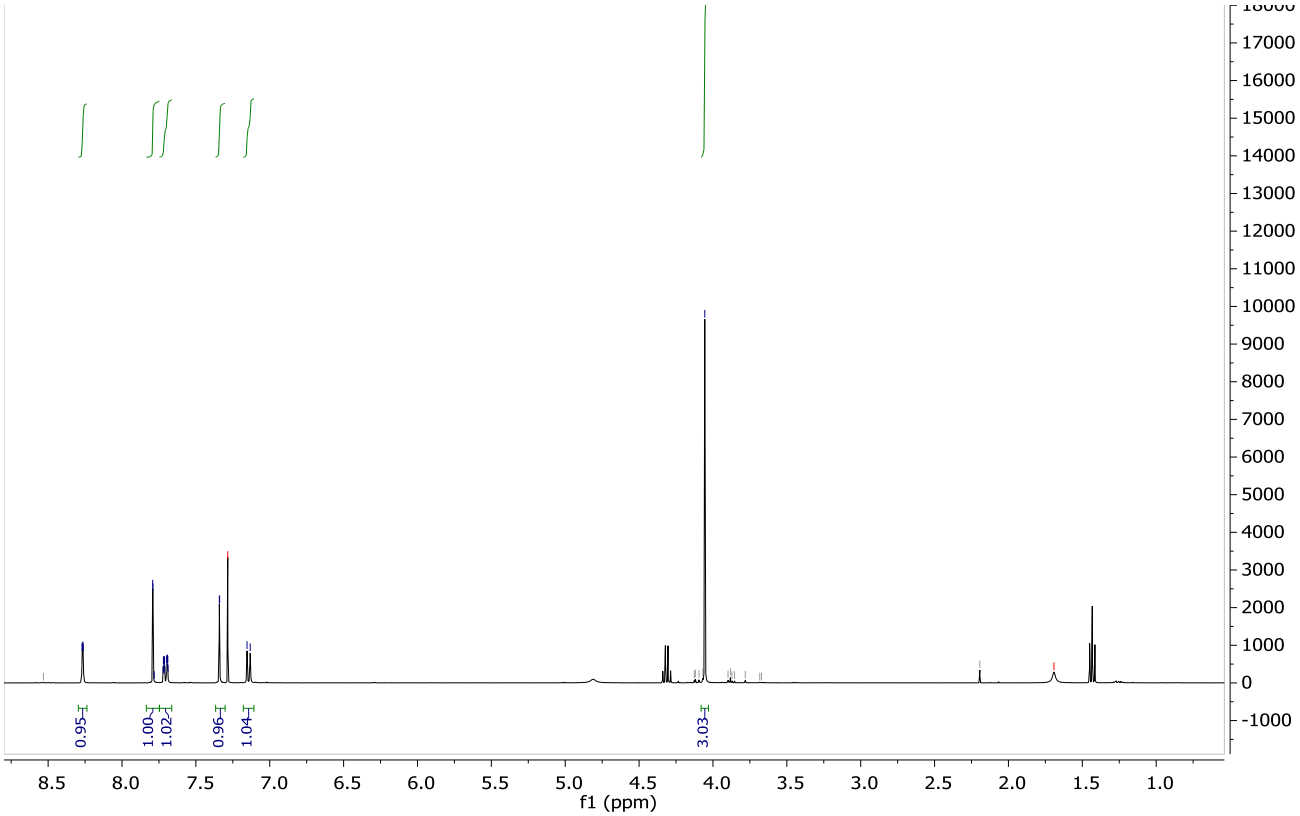

Figure S33. ^{1}H NMR spectrum of **19** in $CDCl_3$.

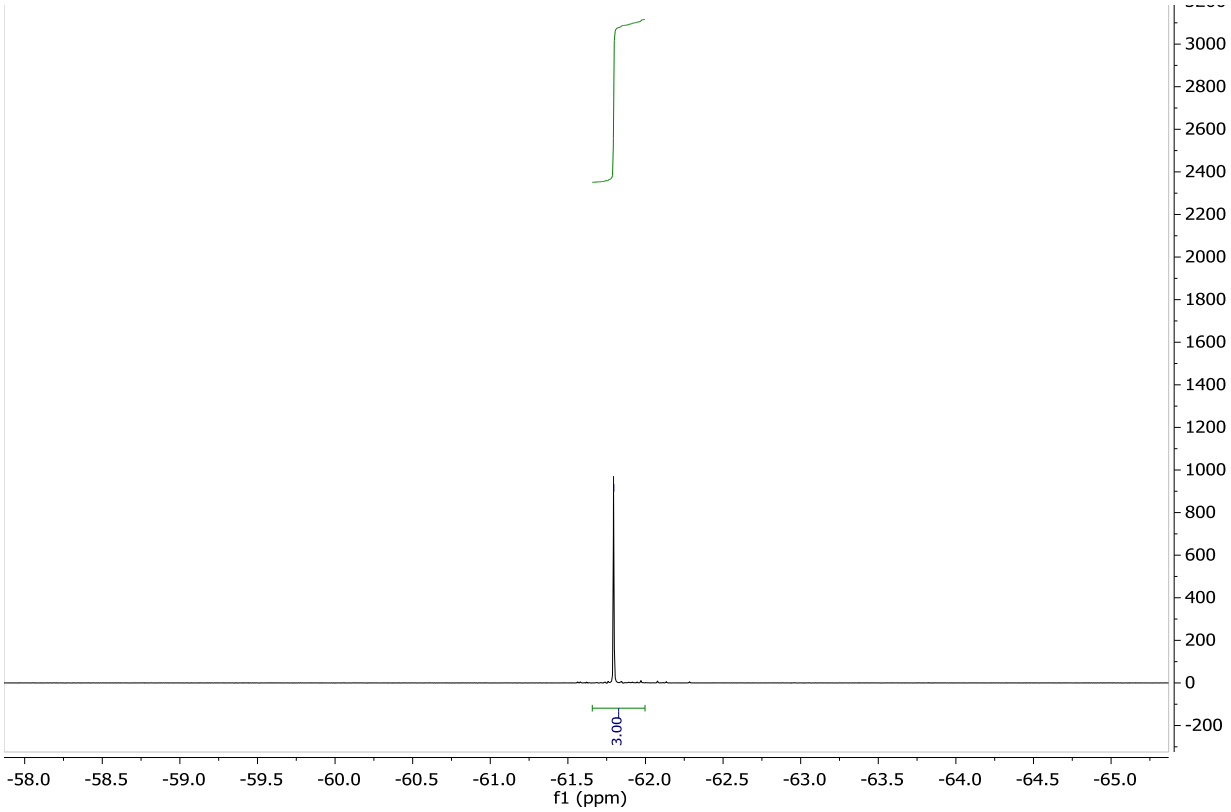

Figure S34. ^{19}F NMR spectrum of **19** in $CDCl_3$.

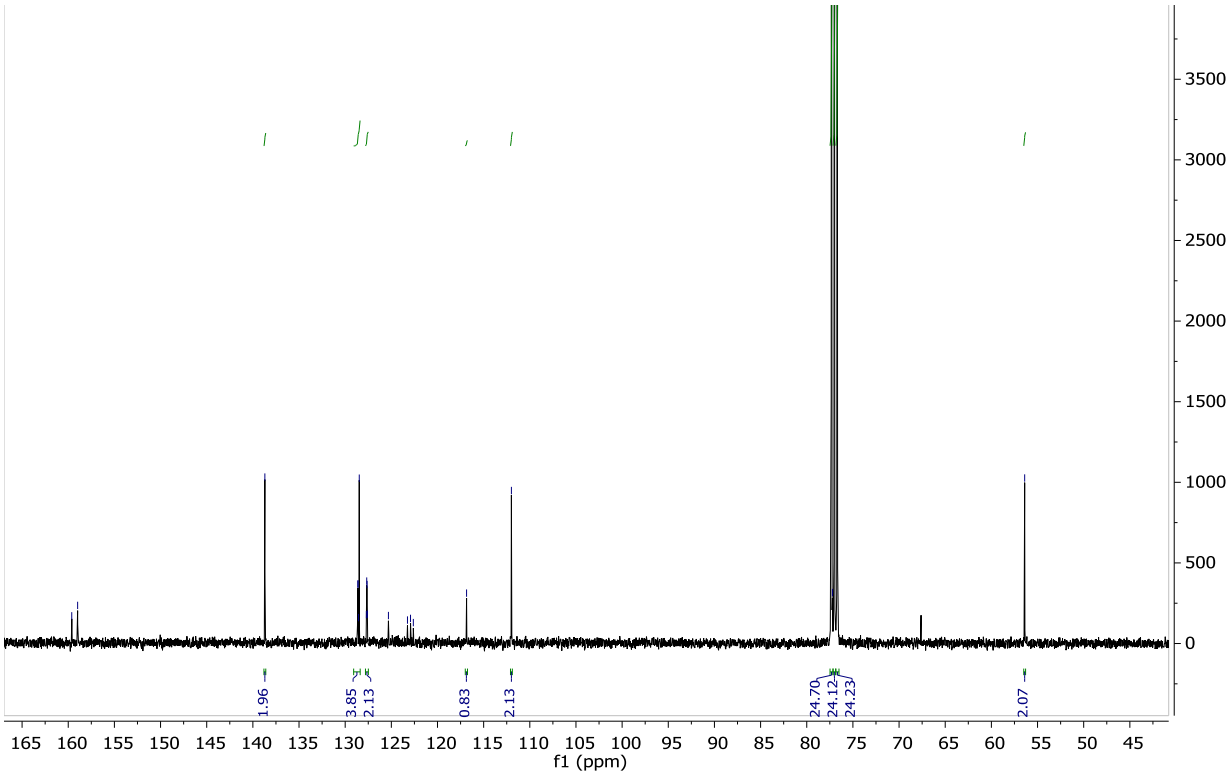

Figure S35. ^{13}C NMR spectrum of **19** in $CDCl_3$.

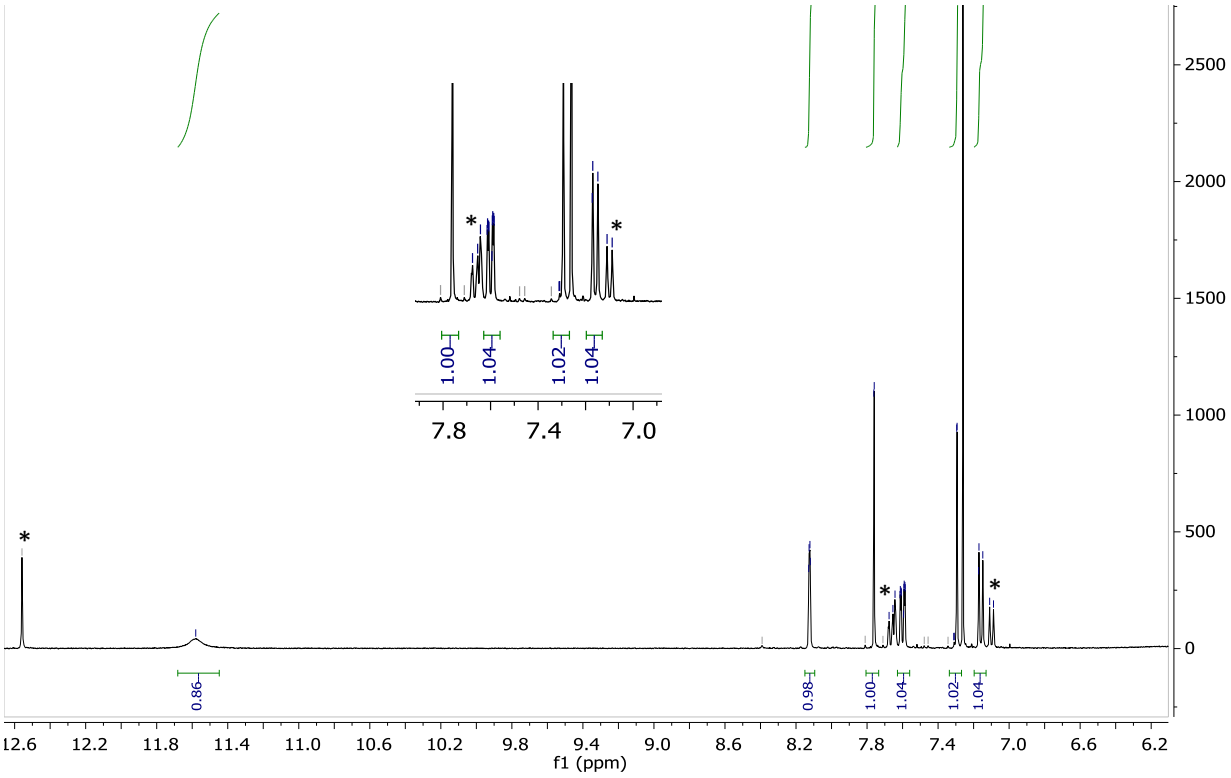

Figure S36. ^{1}H NMR spectrum of **20** in $CDCl_3$. The * denotes peaks from the decomposition product.

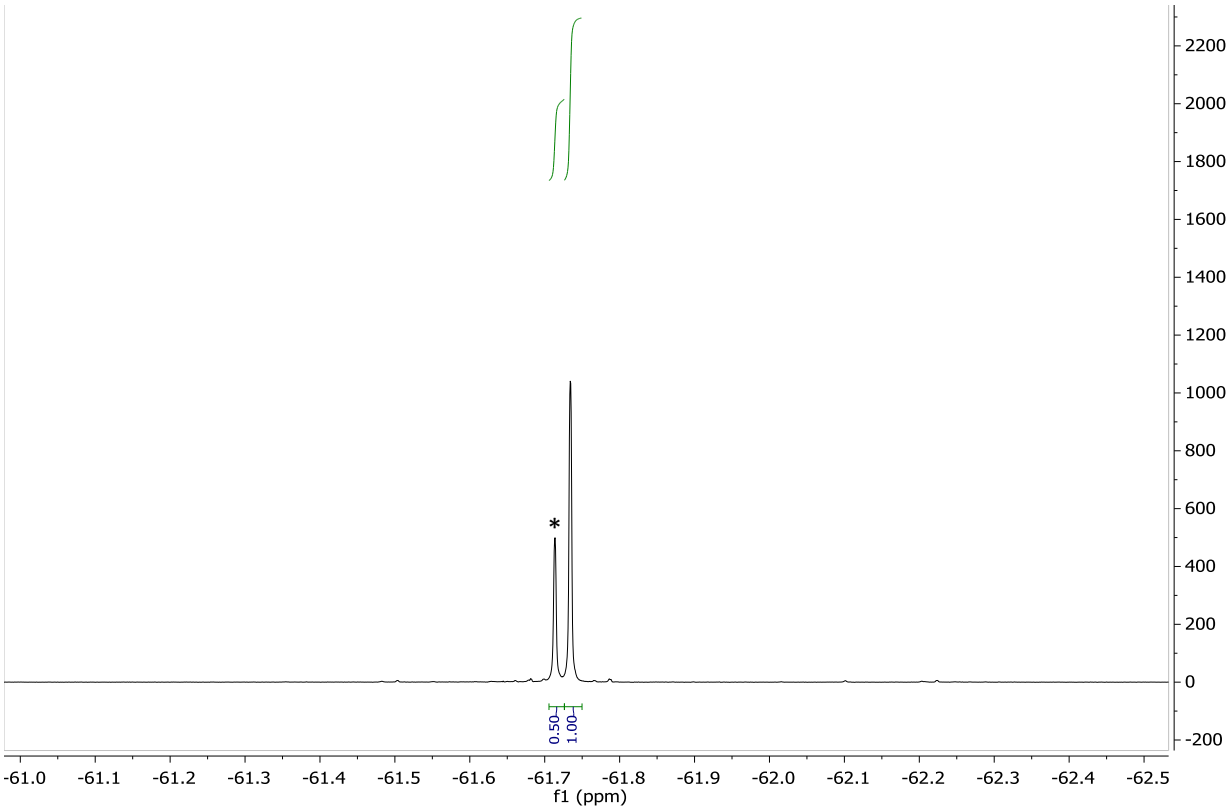

Figure S37. ^{19}F NMR spectrum of **20** in $CDCl_3$. The * denotes peaks from the decomposition product.

Photophysical properties

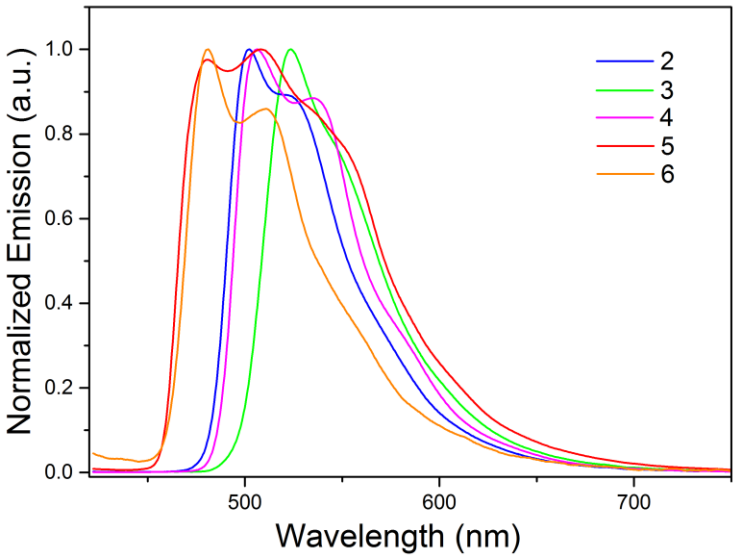

Figure S38. Emission spectra of complexes **2-6** at 77 K in THF solution with λ_{ex} = 365 nm.